systems

MDPI

Article

Assessment of Flood Disaster Resilience in an Urban Historic District Based on G-IC Model

Bo Huang [1,2,3,*], Tsuyoshi Kinouchi [3] and Gang Zhao [3]

[1] Sanya Science and Education Innovation Park, Wuhan University of Technology, Sanya 572025, China
[2] School of Civil Engineering and Architecture, Wuhan University of Technology, Wuhan 430070, China
[3] Department of Transdisciplinary Science and Engineering, Institute of Science Tokyo, Tokyo 145-0061, Japan
* Correspondence: bohuang@whut.edu.cn

Abstract

Urban historic districts play a vital role in shaping the cultural identity and heritage of cities. However, many of these areas face challenges such as aging buildings and deteriorating infrastructure. At the same time, the increasing frequency of extreme rainfall has led to a rise in flood events, placing these vulnerable districts at greater risk. Therefore, it is essential to carry out a comprehensive and objective assessment of their resilience to flood disasters. This study establishes a G-IC model for evaluating the resilience of urban historic districts to flood disasters based on the game combination empowerment-improved cloud model method. The proposed method has been demonstrated in the Soviet-style building complex of the Daye Steel Plant in Huangshi and reveals that the driving force layer exhibits weak resilience; the pressure and state layers show general resilience; the impact and response layers demonstrate weak resilience; and the overall resilience of the district is categorized as weak. The consistency of the results was verified by calculating the cloud similarity, which shows that the constructed new model has certain rationality and feasibility, and the evaluation results are relatively accurate. The findings offer valuable insights for policy-making and support for decision-makers in local government departments.

Keywords: urban historic district; flood disaster; resilience assessment; G-IC model; China

check for updates

Academic Editor: Timothy Ferris

Received: 21 July 2025
Revised: 28 August 2025
Accepted: 12 September 2025
Published: 15 September 2025

Citation: Huang, B.; Kinouchi, T.; Zhao, G. Assessment of Flood Disaster Resilience in an Urban Historic District Based on G-IC Model. *Systems* **2025**, *13*, 809. https://doi.org/10.3390/systems13090809

Copyright: © 2025 by the authors. Licensee MDPI, Basel, Switzerland. This article is an open access article distributed under the terms and conditions of the Creative Commons Attribution (CC BY) license (https://creativecommons.org/licenses/by/4.0/).

1. Introduction

An urban historic district (UHD) refers to a town, street, or village that embodies rich cultural heritage, and holds significant historical or revolutionary importance. As "living fossils" of urban history, these districts vividly represent the form and customs of a city during specific historical periods. They hold immense value in terms of history, culture, art, and science, making them vital areas that embody the unique identity of a city [1–5]. According to the World Meteorological Organization, climate change and human activity have significantly disrupted global water cycles, contributing to the growing frequency of extreme weather events and related disasters. These changes have caused substantial ecological, economic, social, and human losses [6]. As a result of a combination of natural geographical factors, meteorological conditions, ecological vulnerability, and rapid urbanization, urban historic districts are increasingly exposed to flood risks. Due to climate change, the frequency and intensity of natural disasters, including floods, will rise over time. These floods not only pose a growing threat to the urban areas themselves but also to the city's invaluable cultural heritage. Urban historic districts are often densely built, with outdated drainage systems, exacerbating waterlogging and flood risks [7]. Over the

past 40 years, the frequency of rainstorms and floods in central China has steadily increased, with urban historic districts in the region facing particularly severe threats. Consequently, flood prevention and management in these areas have become an urgent priority. Despite growing challenges related to macroeconomic conditions and disaster risk, limited research has focused specifically on flood disaster assessment and protection in urban historic districts [8]. Most existing studies emphasize general disaster risk and the vulnerability of affected populations, while evaluations of historic sites tend to rely on qualitative assessments centered on heritage assets. These approaches often fall short in addressing the practical needs of disaster prevention in historically significant urban areas. Even the few quantitative studies available tend to adopt a disaster science perspective, focusing narrowly on physical vulnerability and indicator-based models [9]. This often overlooks the intrinsic cultural and historical values that define such districts. Current research in flood risk assessment can generally be categorized into four methodological types: historic disaster statistics, remote sensing combined with GIS, indicator-based systems, and scenario simulation. While these approaches contribute valuable insights, they frequently lack integration with heritage-specific considerations essential for comprehensive resilience planning in historic urban settings [10].

Bomers et al. [11] applied an artificial neural network to reconstruct a regional flood hydraulic model by integrating historical flood events into a dataset of annual maximum flow records. This historical disaster statistics approach effectively leverages past flood data for regional risk analysis and offers a straightforward calculation process. However, it relies heavily on the availability of historical records, limiting its applicability in areas with sparse data or small-scale sites. In another study, Aktürk et al. [12] examined rural settlements in the Fındıklı area of Rize, northeastern Turkey. By integrating ArcGIS with georeferenced data on buildings and natural heritage sites, they analyzed spatial planning changes under increasing flood and landslide threats. The coupling of remote sensing technology with GIS allows researchers to map the spatial distribution of flood risks and monitor real-time changes. Yet, this method demands highly accurate ground elevation data, and flood depth analysis in GIS remains technically immature. Pala et al. [13] focusing on Istanbul's Pendik district, employed the AHP using survey and census data to explore the correlation between urban flood exposure and vulnerability. This indicator-based method is versatile across urban scales and effectively clarifies causal relationships among variables. Nevertheless, it lacks the capacity to directly visualize the resilience levels of historic districts. D'Ayala et al. [14] investigated a heritage site in Kuala Lumpur, Malaysia, combining a vulnerability model with high-resolution river and flood inundation maps. They conducted scenario simulations based on annual exceedance probabilities (AEP) greater than 0.1%, and developed damage functions to estimate economic losses at the building level. This method offers both qualitative and quantitative insights, allowing for detailed spatial assessments and multiple scenario analyses. However, it is data-intensive, computationally complex, and requires substantial preparatory work.

The above scholars have conducted certain research on flood risks and vulnerabilities in urban historic districts or heritage areas, but have not mathematically quantified and classified the assessment results, nor presented them intuitively. Therefore, this paper adopts the game combination empowerment-improved cloud model assessment method to establish the G-IC model for resilience assessment of urban historic districts. It can not only present the assessment results intuitively, but also quantitatively classify and verify the results, ensuring the scientific nature of the research. First, an assessment system is established based on the DPSIR theoretical model. The optimal combination weights of G1 and CRITIC are solved through the game theory algorithm, and then the assessment cloud map is drawn in combination with the cloud model assessment method. Finally,

the assessment results are verified through cloud similarity measurement, and the level of flood disaster resilience of urban historic districts is finally obtained. This paper takes the historical district of the Soviet-style building complex of Daye Steel Plant in Huangshi as the research object, and verifies the G-IC model for resilience assessment of urban historic districts. According to the research results, it can be concluded that the assessment model has accuracy and applicability. Assessment Framework Diagram is shown in Figure 1.

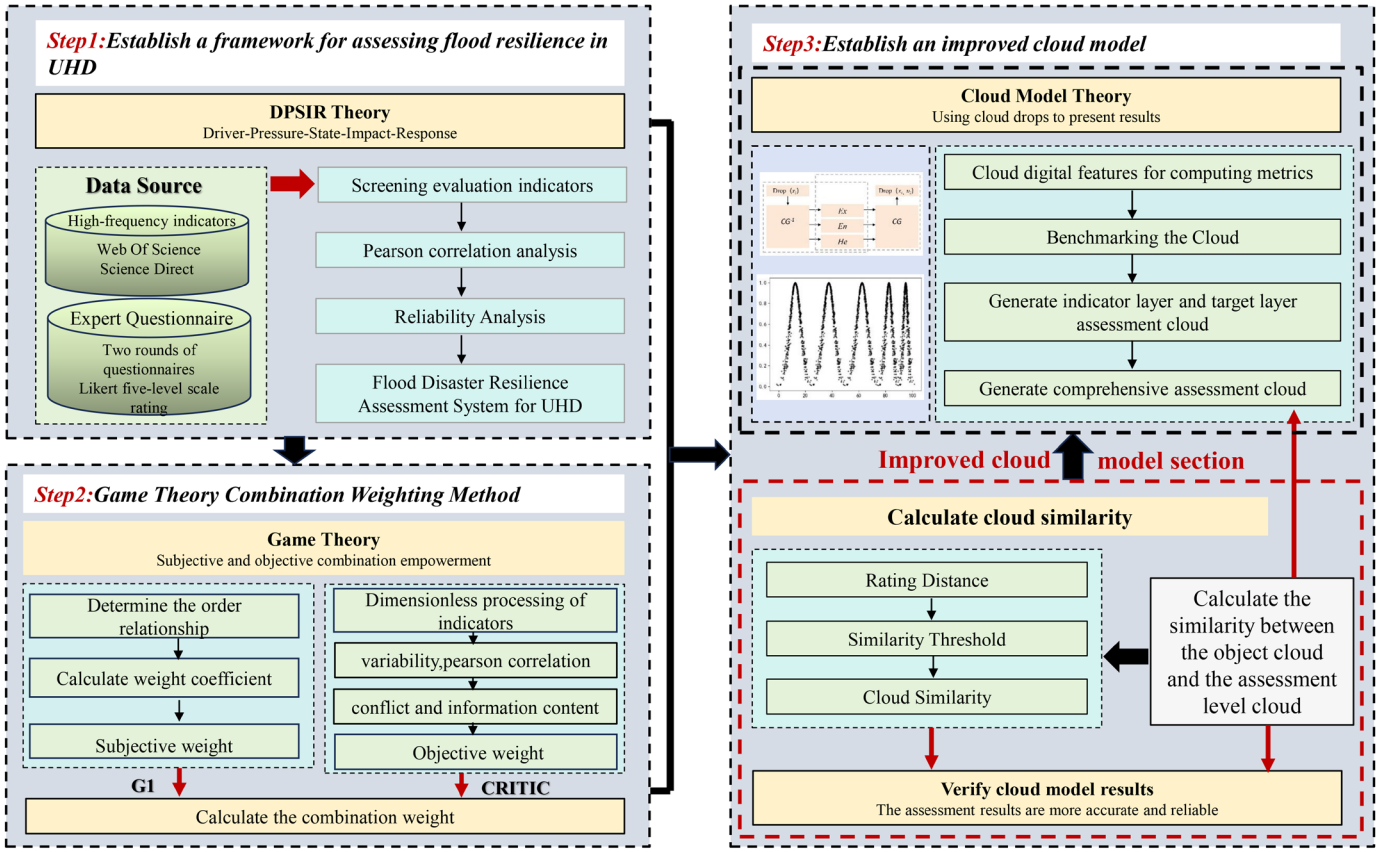


Figure 1. Assessment Framework Diagram.

2. Study Area

The historic district of the Soviet-style building complex of Daye Steel Plant in Huangshi was built in the 1950s. Its architectural style was influenced by the Soviet-style architecture of the time. It is a historic district that combines industrial and residential functions. It carries the glory and memory of Huangshi in the past and has become an important urban landmark in Huangshi. The entire building complex is built on the hillside, with a staggered layout and distinctive environmental characteristics. The design concept and construction technology were at the highest level at the time. The entire historic district is based on production space. The Soviet-style building complex consists of three-story brick and wood structures. The buildings are located on the hillside and are staggered. The red brick sloping roof building of the building complex has a three-section structure of eaves, wall body, and plinth. The plane is symmetrical in the central axis, which is a typical style of Soviet-style architecture and has great historic and aesthetic value. The details of the building are mostly ingeniously constructed, and the overall simplicity, elegance and solemnity are the classic elements of Soviet-style architecture, such as window styles, balcony carvings, hollow shapes, window frames and door frames, as shown in Figure 2.



Figure 2. District environment.

There are 24 Soviet-style buildings in the historic district of the Soviet-style building complex of Daye Steel Plant in Huangshi, with a total land area of 37,123.3 square meters. Among them, buildings 1 to 23 are Soviet-style buildings, covering an area of 9601.9 square meters and a construction area of 28,805.7 square meters. The historic district presents a determinant, high-density, regular and homogeneous spatial texture, and the surrounding new buildings present a large-scale, low-density, rough spatial texture, and the overall spatial coordination is poor. The overall greening environment of the area is good, with lush plants. The public space is mainly composed of the front yard and strip green space, which is pleasant in scale but has a low utilization rate. There is a lack of public space connection with the open space in the city, and the vitality is insufficient. The public space of the block is mainly the landscape square at the entrance, and other areas are mainly strip greening between houses. The overall public activity space is small and the space utilization rate is low.

Through on-site investigation and relevant literature inquiry, it can be found that the historic district of the Soviet-style building complex of Daye Steel Plant in Huangshi is located in a narrow flat land between the mountains, with an "L" shape layout, as shown in Figure 3. The red dotted line in Figure 3 indicates the scope of the historic district studied this time, and the areas marked with yellow circles are the low-lying areas and drainage points of the historic district. The historic district has dense houses and low building elevation. When the rainfall intensity is too high, the water volume in the block increases rapidly, and it is difficult for the internal districts to drain quickly, resulting in waterlogging. Basically, there will be waterlogging every time it rains, and it is a flood prone area. Every time there is a flood, the historic district will suffer from the impact of the flood peak, the scouring damage to the buildings during the water flow, and the flood soaking damage, which will cause great damage to the surrounding buildings, thereby causing the value reduction of material space carriers such as historic buildings, street spaces, clustered areas and characteristic spaces, and directly threatening the safety of residents.



Figure 3. Overall layout of the district.

3. Methodology

3.1. Establish a Flood Risk Assessment System for UHD

3.1.1. Screening of Evaluation Indicators

To identify current research trends and establish relevant assessment indicators, literature was retrieved using research-related keywords in the Web of Science and ScienceDirect databases. This provided insight into prevailing academic focuses and the status of research on the topic. Following a thorough review, frequently cited indicators were initially identified and summarized. A two-round expert questionnaire method was then employed to refine the indicator set. In the first round, experts in related fields were invited to review the preliminary indicators, suggesting modifications through merging, deletion, or supplementation. Their qualitative feedback was systematically analyzed and encoded [15]. Based on these responses, a second-round questionnaire was developed, in which experts evaluated each indicator.

Based on the reliability and validity criteria of the questionnaire, SPSS 27 software was used to conduct Pearson correlation analysis on the indicators in the questionnaire.

The correlation of each indicator was calculated and tested according to Formula (1), and any problems were identified and corrected in a timely manner [16].

$$H = \frac{\sum (X_i - \overline{X})(Y_i - \overline{Y})}{\sqrt{\sum (X_i - \overline{X})^2 \cdot \sum (Y_i - \overline{Y})^2}} \quad (1)$$

$\overline{X}, \overline{Y}$ are the average values of the two questionnaire data.

In the reliability analysis, after removing the four indicators with low correlation, the scale composed of the remaining indicators was further tested [17]. The calculation is shown in Formula (2).

$$\alpha = \frac{e}{e-1}\left(1 - \frac{\sum_{i=1}^{e} \sigma_i^2}{\sigma_{\text{total}}^2}\right) \quad (2)$$

e is the number of indicators in the questionnaire, σ_{total}^2 is the variance of the questionnaire data, and σ_i^2 is the method of collecting data for the *i-th* question.

3.1.2. Flood Risk Assessment System for UHD

Scholars adopting the DPSIR framework typically approach their analyses from its five core dimensions—Driving forces, Pressures, States, Impacts, and Responses—selecting relevant indicators, assigning weight coefficients, and using the model to objectively assess their research subjects. Given its versatility and proven effectiveness [18], the DPSIR model is well-suited for assessing flood disaster resilience in urban historic districts, as proposed in this study.

The DPSIR model is an extension of the earlier PSR (Pressure–State–Response) framework. The PSR model has proven valuable for systematically analyzing the pressures exerted on a system, its current state, and corresponding response strategies [19]. The DPSIR model adds two more criteria layers: driving force and influence, based on the PSR model. Each layer of the DPSIR model comprises multiple indicators, enabling a more nuanced understanding of the interactions between system components and facilitating the simplification of complex problems [20]. Compared to the linear structure of the PSR and DSR models, the DPSIR model offers a more dynamic and integrated approach. As a mature and interdisciplinary ecological assessment framework, DPSIR effectively captures both the stages and capacities of system resilience. Its holistic nature makes it particularly suitable for assessing flood disaster resilience in urban historic districts.

3.2. Game Empowerment Method

Game theory is an operations research method that takes subjective and objective rights as the subjects in the game. Both parties seek a balance of interests in the constant conflict to achieve the optimal weight combination and obtain more accurate weights [21].

3.2.1. G1 Method

Order relationship analysis method is also called G1 method. It is a method for determining subjective weights that is reasonably improved on the basis of analytic hierarchy process [22]. The calculation is simple and has good operability.

1. Determine the order relationship

Determine the unique order relationship from left to right according to the importance [23]. The order relationship of the assessment index x is shown in Formula (3).

$$x_1^* \geq x_2^* \geq \ldots x_m^* \quad (3)$$

2. Calculate the weight coefficient

The relative importance of adjacent indicators is calculated according to Formula (4).

$$r_z = w^*_{(z-1)}/w^*_z \ (z = 2,\ m-1, \ldots, m) \tag{4}$$

where: w^*_{z-1} and w^*_z are the weights of the $z-1th$ and *z-th* indicators respectively. Before calculation, the weight w^*_z is unknown, and r_z can be obtained through expert scoring [24,25]. The value of r_z is shown in Appendix B Table A3.

The weight coefficient of the *z-th* indicator can be obtained according to Formula (5), and the weights of other indicators can be calculated according to Formula (6).

$$w_z = (1 + \sum_{z=2}^{m} \prod_{i=z}^{m} r_z)^{-1} \tag{5}$$

$$w_{z-1} = r_z w_z \quad (z = 2, \ldots, m-1, m) \tag{6}$$

3. Expert group decision-making determines G1 weights

The expert authority coefficient P_r reflects the authority and persuasiveness of the questionnaire. $P_r > 0.7$ is considered statistically significant. A higher authority coefficient indicates a higher persuasiveness of the expert panel. The expert familiarity coefficient P_s and judgment basis coefficient P_d are quantified based on the expert's familiarity with the questionnaire and their judgment basis. The specific calculation is shown in Formula (7).

$$P_r = \frac{P_s + P_d}{2} \tag{7}$$

If n experts rank and judge the indicators, the weight assigned to the indicators by each expert, w_n, is calculated according to the above formula [26]. Combining the expert's assigned weight and the indicator weight, the final weight of the *z-th* indicator of the G1 method is calculated using Formula (8) as w_{fz}.

$$w_{fz} = \sum_{n=1}^{n} w_n w_z \tag{8}$$

3.2.2. CRITIC Method

CRITIC is an objective weighting method that comprehensively considers the weight of indicators based on the comparison strength and conflict between indicators [27–29]. Establish an assessment matrix with m evaluation samples and n influencing factors as indicators, as shown in Formula (9).

$$X_{ij} = \begin{bmatrix} x_{11} & x_{12} & \ldots & x_{1n} \\ x_{21} & x_{22} & \ldots & x_{2n} \\ \vdots & \vdots & \ldots & \vdots \\ x_{m1} & x_{m2} & \ldots & x_{mn} \end{bmatrix} \tag{9}$$

1. Each index is dimensionless and can be calculated using Formula (10).

$$\begin{cases} y_{ij} = \frac{x_{ij} - \min(x_j)}{\max(x_j) - \min(x_j)} & \text{(Positive indicators)} \\ y_{ij} = \frac{\max(x_j) - x_{ij}}{\max(x_j) - \min(x_j)} & \text{(Negative indicators)} \end{cases} \tag{10}$$

x_{ij} represents the *j-th* indicator of the *i* object to be evaluated, y_{ij} represents the standardized indicator value.

2. Calculate the comparative strength of the quantitative index of index variability according to Formula (11).

$$B_j = \sqrt{\frac{\sum_{i=1}^{m}(\quad y_{ij} \quad -\overline{y}_j \quad)^2}{N \quad - \quad 1}} (i = 1, 2, \ldots, m; j = 1, 2, \ldots, n) \tag{11}$$

$\overline{y}_j$ is the average of the indicators; N is the number of indicators.

3. Calculate the Pearson correlation, remove the assessment indicators with high correlation, and calculate according to Formula (12).

$$U_{ij} = \frac{\sum_{k=1}^{m}\left(y_{ki}^{*} - \overline{y_i^{*}}\right)\left(y_{kj}^{*} - \overline{y_j^{*}}\right)}{\sqrt{\sum_{k=1}^{m}\left(y_{k_i}^{*} - \overline{y_i^{*}}\right)^2}\sqrt{\sum_{k=1}^{N}\left(y_{kj}^{*} - \overline{y_j^{*}}\right)^2}} \tag{12}$$

y_{ki}^{*}, y_{kj}^{*} are the standardized values of the *i-th* and *j-th* assessment indicators of the k assessment objects; $\overline{y_i^{*}}$, $\overline{y_j^{*}}$ are their average values.

4. According to Formulas (13) and (14) calculate the index conflict V_j and information volume C_j.

$$V_j = \sum_{i=1}^{n}(1 - |U_{ij}|)(i \neq j) \tag{13}$$

The correlations between i and j with the same absolute values can reflect the same indicator correlations.

$$C_j = \frac{\sigma_j}{\overline{y}_j}\sum_{i=1}^{n}(1 - |U_{ij}|) \tag{14}$$

n represents the number of assessments made by an expert on the same indicator; $\sigma_j = \sqrt{\sum_{j=1}^{n}\left(y_{ij} - \overline{y}_{ij}\right)^2}$ is the standard deviation of the *j-th* assessment indicator.

5. According to Formula (15) the final weight of the *j-th* indicator of the CRITIC method is calculated as w_j.

$$w_j = \frac{C_j}{\sum_{j=1}^{n} C_j} \tag{15}$$

3.2.3. Game Empowerment

In order to reduce the deviation between weights and increase the accuracy of the indicator weight calculation results, this study calculated the optimal combination coefficient of the subjective and objective weighting algorithm based on the game theory combined weighting formula, and then obtained the weights of each indicator after integration [30–33].

The linear coefficient of the optimized combination weight is calculated according to Formulas (16)–(19)

$$A = \sum_{k=1}^{g} b_k A_k^T \tag{16}$$

$b_1, b_2, \ldots, b_k$ are the weight combination coefficients of each weighting method, A_k is the set of k weighting methods, g is the number of weight calculation methods, A_k^T is the transposed matrix of A_k.

$$\min\left\|\sum_{k=1}^{g} b_k A_k^T - \quad A_k\right\|_2 \quad (k = 1, 2, \ldots, \ g) \tag{17}$$

$$\begin{bmatrix} A_1A_1^T & A_1A_2^T & \cdots & A_1A_g^T \\ A_2A_1^T & A_2A_2^T & \cdots & A_2A_g^T \\ \cdots & \cdots & \cdots & \cdots \\ A_gA_1^T & A_gA_2^T & \cdots & A_gA_g^T \end{bmatrix} \cdot \begin{bmatrix} b_1 \\ b_2 \\ \cdots \\ b_L \end{bmatrix} = \begin{bmatrix} A_1A_1^T \\ A_2A_2^T \\ \cdots \\ A_gA_g^T \end{bmatrix} \tag{18}$$

$$b_k^* = b_k \Big/ \sum_{k=1}^{g} b_k \tag{19}$$

According to Formula (20), the combined weight A^* can be calculated.

$$A^* = \sum_{k=1}^{g} b_k^* A_k^T \tag{20}$$

3.3. Improved Cloud Model

Cloud model theory takes into account the randomness and fuzziness of the indicators and uses cloud drops to present them intuitively and concretely, which has an absolute advantage in the analysis of complex systems [34]. The cloud model is verified by calculating the cloud similarity to obtain an improved cloud model [35–38].

3.3.1. Cloud Digital Features of Calculation Indicators

A specific algorithm is used to show that the random variables, namely cloud droplets, obey the pan-normal distribution, and the fuzzy concept is described with the help of probability theory [39–41]. The cloud digital characteristics of the evaluation index x_i are calculated by Formulas (21)–(24).

1. The sample mean E_x can be calculated using Formula (21).

$$E_x = \overline{X} = \frac{1}{n}\sum_{i=1}^{n}(x_i) \tag{21}$$

2. The sample variance can be calculated according to Formula (22).

$$s^2 = \frac{1}{n-1}\sum_{i=1}^{n}(x_i - \overline{X}) \tag{22}$$

3. Calculate the cloud droplet entropy En according to Formula (23).

$$E_n = \sqrt{\frac{\pi}{2}} \times \frac{1}{n}\sum_{i=1}^{n}|x_i - E_x| \tag{23}$$

4. Calculate the excess entropy He of cloud droplets according to Formula (24).

$$H_e = \sqrt{|s^2 - En^2|} \tag{24}$$

3.3.2. Determine the Standard Evaluation Cloud

The indicator assessment domain is divided into l sub-intervals, and the standard assessment cloud is calculated according to Formula (25).

$$\begin{cases} Ex_i &= \frac{l_i^{min} + l_i^{\max}}{2} \\ En_i &= \frac{l_i^{min} - l_i^{\max}}{2\sqrt{21n2}} \\ H_{e_i} &= k \end{cases} \tag{25}$$

In this paper, $k = En_i/10$ is taken.

3.3.3. Generate Indicator Layer, Criterion Layer and Comprehensive Layer Assessment Cloud

The lowest and highest cloud digital features (Ex_C^{min}, En_C^{min}, He_C^{max}), (Ex_C^{max}, En_C^{max}, He_C^{max}) are calculated respectively, and the comprehensive cloud model digital features (Ex_c, En_c, He_c) of each indicator are calculated through the comprehensive cloud generator. The algorithm is shown in Formulas (26) and (27) [42,43].

$$\begin{cases} Ex_c = & \frac{Ex_c^{min} En_c^{min} + Ex_c^{max} En_c^{\max}}{En_c^{min} + En_c^{\max}} \\ En_c = & En_c^{min} + En_c^{max} \\ He_c = & \frac{He_c^{min} En_c^{min} + He_c^{max} En_c^{\max}}{En_c^{min} + En_c^{\max}} \end{cases} \tag{26}$$

$$\begin{cases} Ex_B = & \frac{\sum_{j=1}^{n} Ex_C A^*}{\sum_{j=1}^{n} A^*} \\ En_B = & \frac{\sum_{j=1}^{n} En_C (A^*)^2}{\sum_{j=1}^{n} (A^*)^2} \\ He_B = & \frac{\sum_{j=1}^{n} He_C (A^*)^2}{\sum_{j=1}^{n} (A^*)^2} \end{cases} \tag{27}$$

The comprehensive assessment cloud digital features are calculated by Formula (28) based on the combined weights of the assessment indicators and the cloud digital features, and then the assessment cloud map is obtained through the cloud generator [44].

$$\begin{cases} Ex = & \frac{\sum_{i=1}^{n} \sum_{j=1}^{n} Ex_C A^*}{\sum_{i=1}^{n} \sum_{j=1}^{n} A^*} \\ En = & \frac{\sum_{i=1}^{n} \sum_{j=1}^{n} En_C \left(A^*\right)^2}{\sum_{i=1}^{n} \sum_{j=1}^{n} \left(A^*\right)^2} \\ He = & \frac{\sum_{l=1}^{n} \sum_{j=1}^{n} He_c \left(A^*\right)^2}{\sum_{i=1}^{n} \sum_{j=1}^{n} \left(A^*\right)^2} \end{cases} \tag{28}$$

3.3.4. Calculating Cloud Similarity

The similarity method is more accurate than intuitively judging the result based on the position of the comprehensive cloud in the reference cloud. When the entropy and super entropy values are large, that is, the cloud droplets are relatively discrete, the model stability is poor. Therefore, similarity measurement is very necessary [45].

1. The distance Q_i between the comprehensive assessment level and the benchmark assessment level is calculated by Formula (29).

$$Q_i = \sqrt{A^*{}_{Ex}(Ex - Ex_i)^2 + A^*{}_{En}(En - En_i)^2 + A^*{}_{He}(He - He_i)^2} \tag{29}$$

2. According to Formula (30), the cloud similarity threshold δ_i is calculated

$$\delta_i = \frac{1}{Q_i} \tag{30}$$

3. According to Formula (31), the cloud similarity l_i is calculated.

$$l_i = \left(\frac{\delta_i}{\sum_{i=1}^{n} \delta_i} \right) \times 100\% \tag{31}$$

By calculating the similarity through the above steps, the actual assessment results can be made more objective [46].

4. Results

4.1. Results of the Flood Risk Assessment System for UHD

4.1.1. Indicator Screening Structure

The questionnaire was filled out online using the "Wenjuxing" platform. The detailed information of the questionnaire is shown in Appendix A. In the first round, a total of 100 questionnaires were distributed, and 93 were effectively collected. Invalid questionnaires included: 4 questionnaires with serious missing items and 3 questionnaires filled out carelessly. In the second round, 100 questionnaires were distributed, with 95 valid responses collected. Three questionnaires were invalid due to significant missing items and two questionnaires were filled out carelessly. The respondents included university researchers, as well as practitioners from design institutes, emergency departments and research institutions. The occupations, areas of expertise, and years of work experience of the experts who responded to the questionnaires are shown in Table 1.

Table 1. Expert information.

Expert Features		First Round of Numbers	Proportion	Second Round of Numbers	Proportion
Experience	Up to 5 years	28	30.1%	24	25.3%
	5–10 years	26	28%	31	32.6%
	More than 10 years	39	41.9%	40	42.1%
Expertise in	Flood resilience	30	32.2%	36	37.9%
	Flood management	42	45.2%	39	41.0%
	Historic district protection	21	22.6%	20	21.1%
Job occupation	University teachers	37	39.8%	37	38.9%
	Design Institute	25	26.9%	13	13.7%
	Emergency departments	31	33.3%	45	47.4%

To more comprehensively reflect the experts' information in the questionnaire, we compiled statistics on their professional titles and ages. This is shown in Figure 4. Figure 4a shows the professional title and age distribution of experts in the first round of questionnaires, while Figure 4b shows the professional title and age distribution of experts in the second round of questionnaires. As can be seen from Figure 4, the experts' ages are mostly concentrated in the 30–50 age range.

According to Formulas (1) and (2), the results of calculating the Pearson correlation of the indicators showed that the Pearson correlation coefficients of the four indicators "Cultural uniqueness", "The proportion of secondary output value", "Building Materials" and "Authenticity" were all lower than 0.4, and the Cronbach's Alpha values were all lower than 0.8, as shown in Figure 5. This shows that the significant correlation level with the total score of the scale is low. Based on theoretical analysis and practical significance, it can be considered that the impact of these four items on the resilience of urban historic districts to flood disasters is relatively limited, and their measurement significance has a certain degree of duplication with other indicators. After comprehensive consideration, this study intends to delete the above four indicators to optimize the construction and measurement efficiency of the scale.

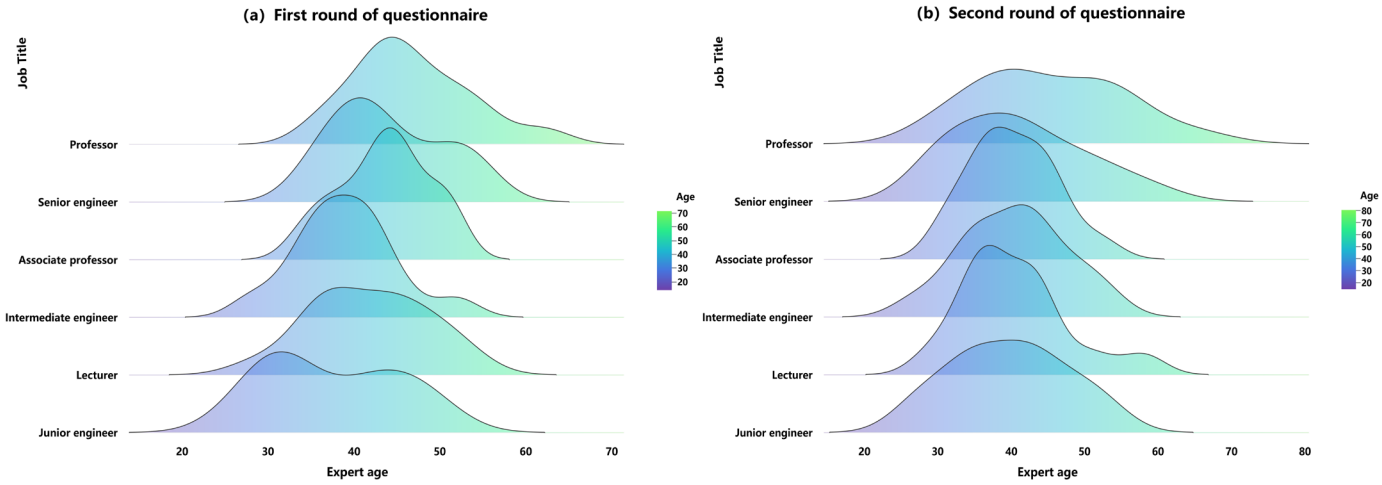


Figure 4. Job title and age distribution of experts in the two rounds of questionnaires.

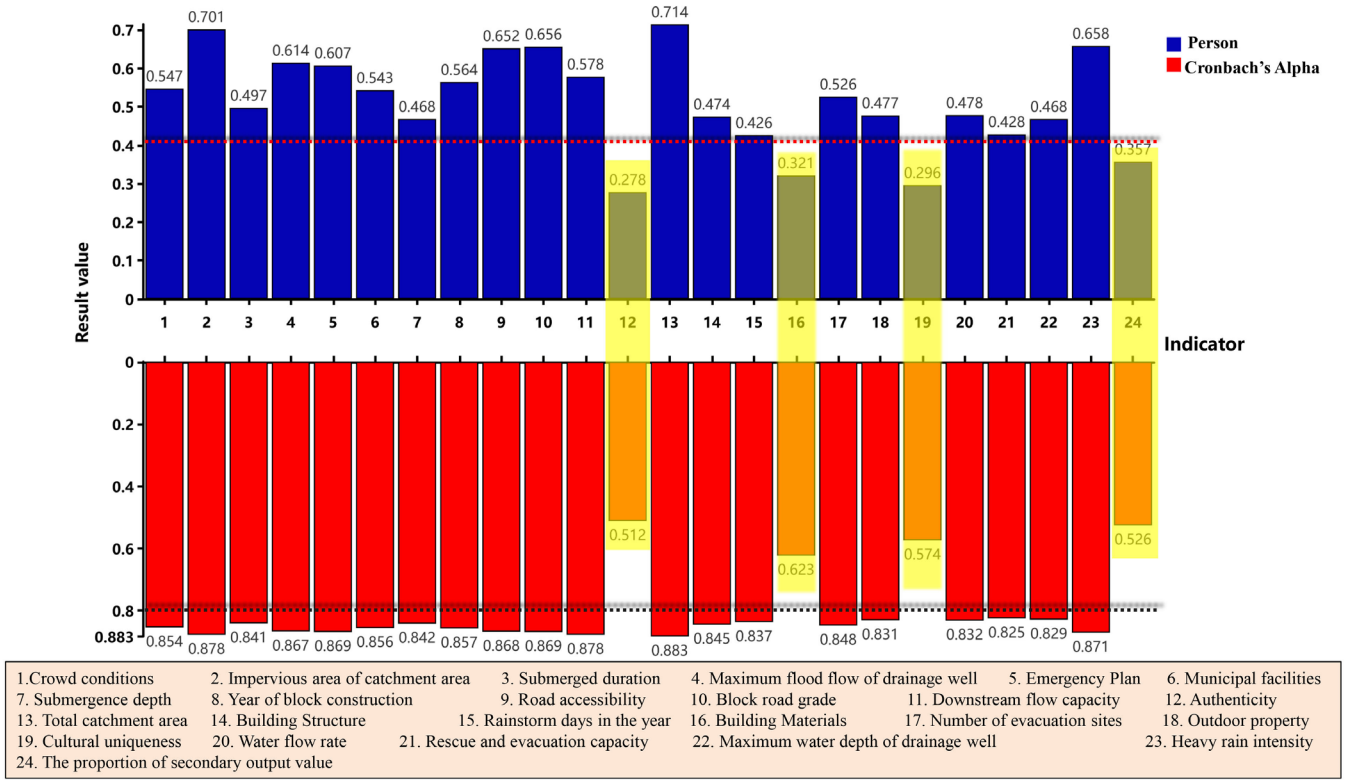


Figure 5. Index test.

After deleting the four indicators with low correlation, the scale consisting of the remaining 20 indicators was further tested. The internal consistency of the optimized scale was not affected and it still maintained a high reliability level. After removing the low-correlation indicators, the scale can still effectively measure the characteristics of the research subjects and ensure overall stability and reliability. Therefore, the scale has good reliability and robustness.

4.1.2. Assessment System

Based on the assessment indicators determined above and combined with the DPSIR model, an urban historic district flood risk assessment index system was established. The assessment system divides the indicators into five levels, as shown in Table 2.

Table 2. Index system for assessing flood disaster resilience in UHD.

Criteria Layer	Indicator Layer	Symbol
Driving force	Crowd conditions	D_1
	Year of block construction	D_2
	Rainstorm days in the year	D_3
	Municipal facilities	D_4
Pressure	Heavy rain intensity (mm/min)	P_1
	Submerged duration (min)	P_2
	Submergence depth (m)	P_3
	Water flow rate (m/s)	P_4
State	Impervious area of catchment area (m^2)	S_1
	Maximum water depth of drainage well (m)	S_2
	Total catchment area (m^2)	S_3
	Block road grade	S_4
Influence	Overcurrent capacity	I_1
	Outdoor property	I_2
	Road accessibility	I_3
	Building Structure	I_4
Response	Maximum flood flow of drainage well (m^3/s)	R_1
	Rescue and evacuation capacity	R_2
	Emergency Plan	R_3
	Number of evacuation sites	R_4

4.2. Results of Game Combination Weighting

4.2.1. G1 Results

1. Determine the order relationship

According to the assessment system established in Section 3.1.2, five experts were invited to use the ordinal relationship method to rank the importance of the assessment indicators at the criterion level and the indicator level. The expert questionnaire information is shown in Appendix B. The importance relationship ranking of the indicator systems of the Huangshi Daye Steel Plant Soviet-style building complex historic district was obtained by Formula (3), as shown in Table 3.

Table 3. Ranking of indicators.

Index	Expert 1	Expert 2	Expert 3	Expert 4	Expert 5
Criteria Layer	S > I > R > D > P	R > S > P > D > I	I > S > P > D > R	P > R > S > I > D	R > S > I > P > D
D	$D_4 > D_3 > D_1 > D_2$	$D_2 > D_4 > D_3 > D_1$	$D_3 > D_4 > D_1 > D_2$	$D_3 > D_2 > D_4 > D_1$	$D_4 > D_3 > D_2 > D_1$
P	$P_3 > P_1 > P_4 > P_2$	$P_1 > P_2 > P_4 > P_3$	$P_3 > P_2 > P_1 > P_4$	$P_2 > P_1 > P_3 > P_4$	$P_3 > P_1 > P_2 > P_4$
S	$S_2 > S_3 > S_4 > S_1$	$S_3 > S_1 > S_2 > S_4$	$S_2 > S_1 > S_3 > S_4$	$S_3 > S_2 > S_4 > S_1$	$S_2 > S_3 > S_1 > S_4$
I	$I_2 > I_3 > I_1 > I_4$	$I_3 > I_1 > I_2 > I_4$	$I_1 > I_2 > I_4 > I_3$	$I_3 > I_1 > I_4 > I_2$	$I_1 > I_3 > I_2 > I_4$
R	$R_2 > R_3 > R_4 > R_1$	$R_1 > R_3 > R_2 > R_4$	$R_3 > R_2 > R_1 > R_4$	$R_2 > R_1 > R_4 > R_3$	$R_1 > R_2 > R_3 > R_4$

2. Calculate the weight coefficient

Experts conduct scientific comparisons on the ranked indicators, and the importance ratio of each indicator is r_{kn}, $k = m - 1, \ldots, 3, 2$. The value of r_{kn} is selected from 1.0 to 1.8

according to the importance ratio, as shown in Appendix B. The greater the difference in importance, the greater the value.

The weight coefficients of each indicator system of the historic district of the Soviet-style building complex of Daye Steel Plant in Huangshi are calculated by Formulas (4)–(6), as shown in Figure 6. According to Figure 5, in the target layer, the weight coefficient of D is the smallest, and the weight coefficient of S is the largest. In the indicator layer, the ones with the largest weight coefficients are D_3, P_3, S_2, I_3, and R_2 respectively. The weights with the smallest coefficients are D_2, P_4, S_4, I_4 and R_4 respectively.

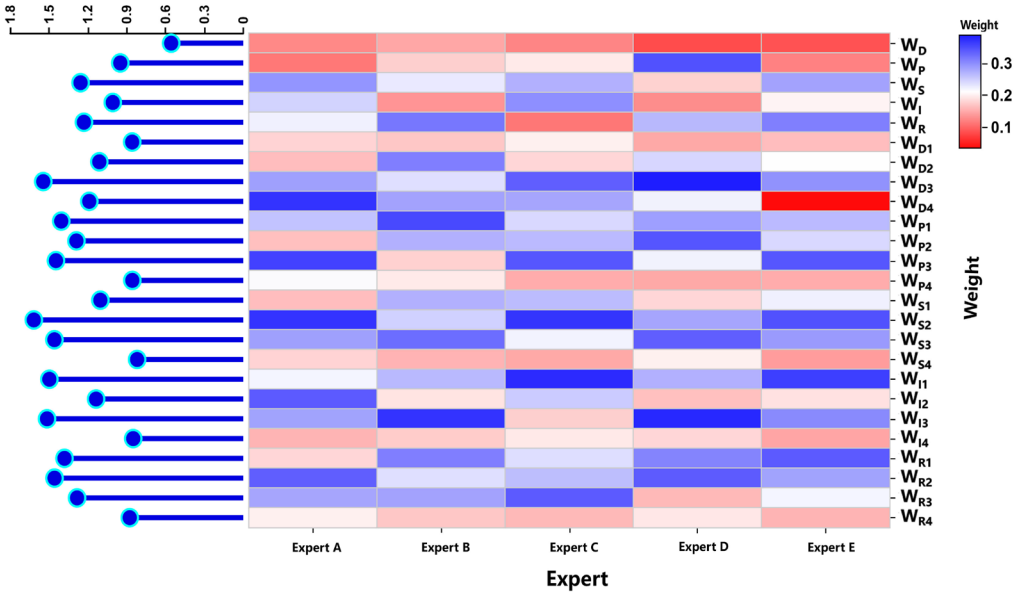


Figure 6. Weight coefficient.

3. Weights under expert group decision making

The coefficients P_s for the familiarity of the experts with the questionnaire were 0.88. The experts' familiarity with the questionnaire is shown in Table 4.

Table 4. Quantitative calculation table of familiarity.

Degree of Understanding	Unfamiliar	Not Very Familiar	General Familiarity	Familiar	Very Familiar
Number	0	0	1	1	3
Familiarity weight	0.2	0.4	0.6	0.8	1

The scores P_d of the expert judgment were 0.94. The experts' familiarity with the questionnaire and the basis for judgment are shown in Table 5.

Therefore, according to Formula (7), the authority coefficients of the experts are 0.91, which shows that the experts have a high degree of authority.

In order to reduce the error of subjective analysis, the weight coefficient of each expert for a certain assessment index is calculated to make the weight result more reasonable and accurate. The expert weights are shown in Table 6.

Table 5. Quantitative calculation table of the judgment.

Judgment Basis	Large		Medium		Small		Fraction
	Number	Assignment	Number	Assignment	Number	Assignment	
Practical experience	3	0.5	2	0.4	0	0.3	0.46
Theoretical analysis	4	0.3	1	0.2	0	0.1	0.28
Field understanding	0	0.1	3	0.1	2	0.1	0.1
Intuition	0	0.1	4	0.1	1	0.1	0.1

Table 6. Weight coefficients of expert assessment.

Expert	Education	Job Title	Length of Service	Familiarity	Score	Weight
Expert 1	1	1	1	3	6	0.0811
Expert 2	3	3	3	3	12	0.1622
Expert 3	1	3	6	6	16	0.2162
Expert 4	6	3	1	6	16	0.2162
Expert 5	6	6	6	6	24	0.3243

After considering the expert's weight coefficient, the weight of the assessment index is calculated and sorted out according to Formula (8), and finally the weighted result of the G1 method of flood disaster resilience assessment index body of Huangshi Daye Steel Plant Soviet-style building complex historic district is obtained, as shown in Figure 7.

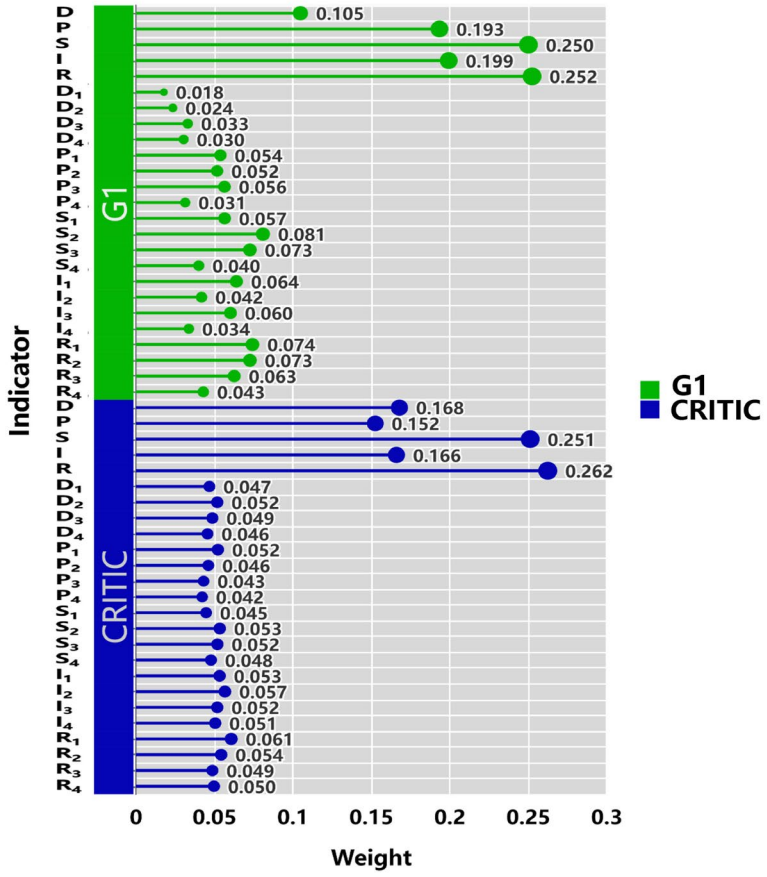


Figure 7. Weights of G1 and CRITIC.

The green part in Figure 7 represents the weight result obtained by the G1 method. It can be seen that in the criterion layer indicators, R has the largest weight and D has the smallest weight. In the indicator layer, S_2 has the largest weight and D_1 has the smallest weight. In the indicator D layer, the weights are D_3, D_4, D_2, and D_1 from large to small. In the indicator P layer, the weights are P_3, P_1, P_2, and P_4 from large to small. In the indicator S layer, the weights are S_2, S_3, S_1, and S_4 from large to small. In the indicator I layer, the weights are I_1, I_3, I_2, and I_4 from large to small. In the indicator R layer, the weights are R_1, R_2, R_3, and R_4 from large to small.

4.2.2. CRITIC Results

1. Dimensionless processing of each index

Based on the assessment and scoring of the real situation of the historic district of the Soviet-style building complex of Daye Steel Plant in Huangshi by different experts as the original data source of the CRITIC method, the index data is standardized to eliminate the impact of the dimension and order of magnitude on the index. In the processing process, positive indicators are processed positively, and negative indicators are processed inversely. The data is standardized according to Formula (10), and the standardized data table is shown in Figure 8a.

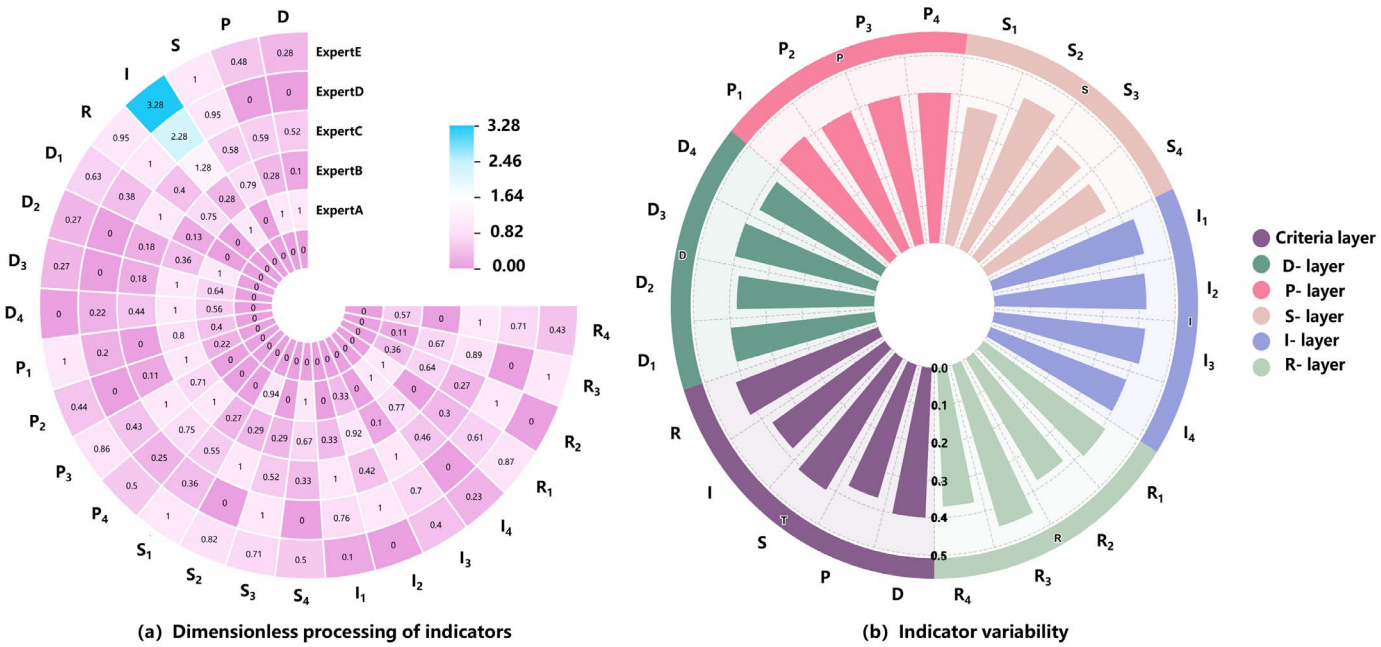


Figure 8. Dimensionless processing of indicators and variability.

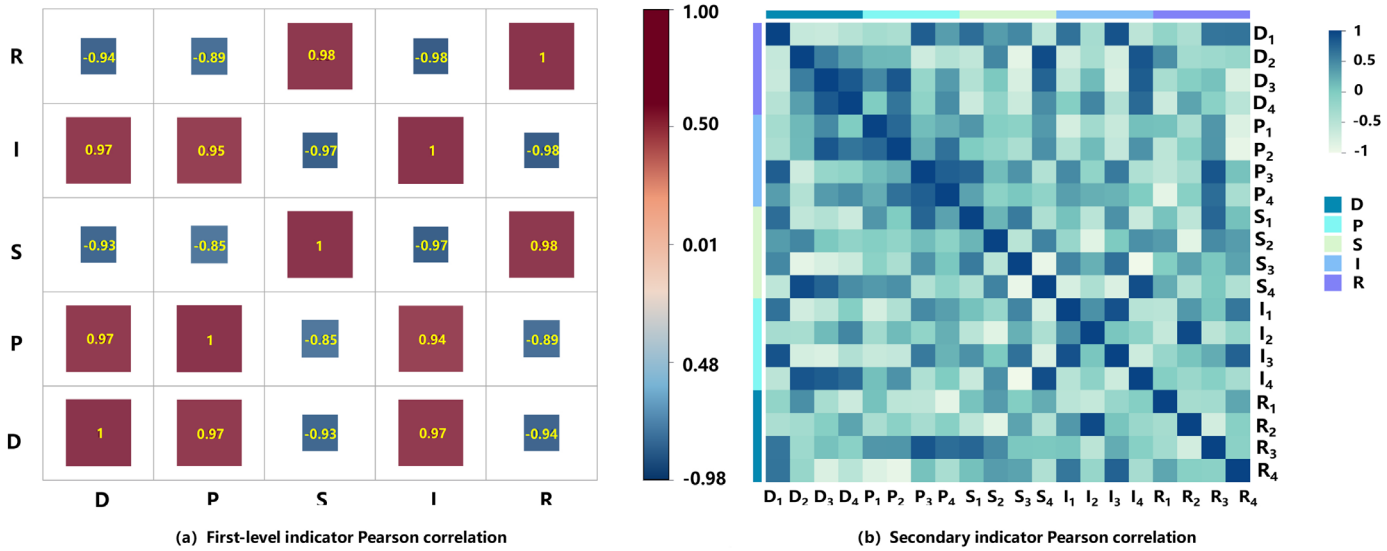
2. Calculation of indicator variability

The indicator variability is calculated according to Formula (11). As can be seen from Figure 8b, the variability of the state (S) in the criterion layer is the largest, the variability of D_3 in the driving force layer is the largest, the variability of P_1 in the pressure layer is the largest, the variability of S_2 in the state layer is the largest, the variability of I_1 in the influence layer is the largest, and the variability of R_3 in the response layer is the largest.

3. Calculation of Pearson correlation

Pearson correlation is used to reveal the strength of the correlation between various assessment indicators. The Pearson correlation of the indicators is calculated according to Formula (12). The calculation results are shown in Figure 9. Figure 9a shows that the larger the red square of the first-level indicator, the stronger the correlation of the indicator.

Figure 9b shows that the greener the color of the indicator in the second-level indicator, the stronger the correlation of the indicator.



(a) First-level indicator Pearson correlation (b) Secondary indicator Pearson correlation

Figure 9. Indicator Pearson correlation.

4. Calculation of index conflict and information content

The stronger the index conflict, the richer the information contained in the scoring result of the index. The greater the information carrying capacity of the index, the richer the information carried by the index, which implies that the relative importance of the index is higher. According to Formulas (13) and (14) the conflict V_j of each index and the information content C_j of each index can be obtained. It can be seen from Figure 10 that R_1 has the largest index conflict and information content, while P has the smallest index conflict and information content.

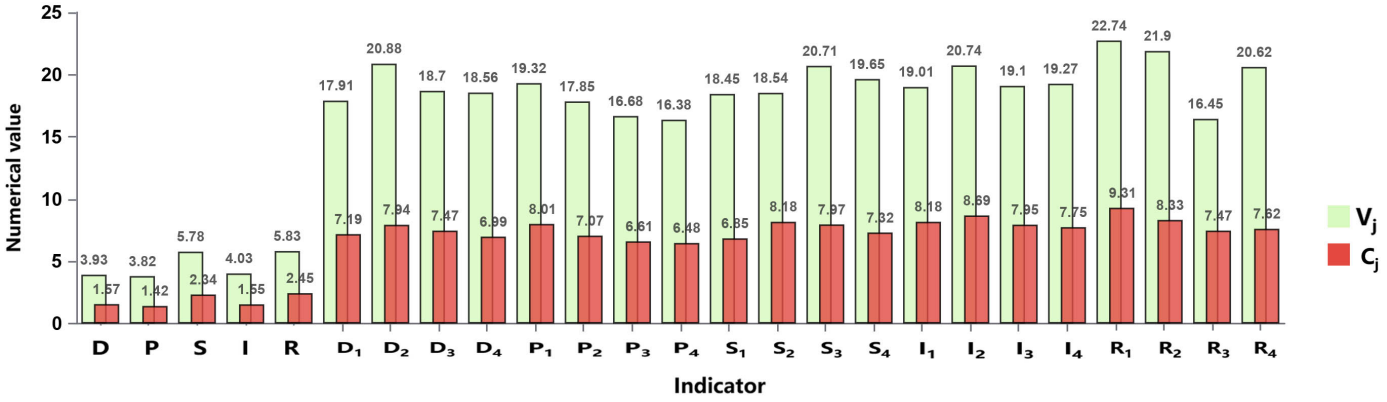


Figure 10. Indicator conflict and information content.

5. CRITIC weight

The indicator weights obtained by the CRITIC method are calculated according to Formula (15). The blue part in Figure 7 represents the weight results obtained by the CRITIC method. It can be seen that among the criterion layer indicators, R has the largest weight and P has the smallest weight. In the indicator layer, R_1 has the largest weight and P_4 has the smallest weight.

From Figure 7, we can conclude that the subjective and objective weight values of S and P_1 are relatively consistent, and the subjective weight values are relatively balanced,

which makes it impossible to highlight the importance of some indicators. The weight values of the remaining indicators vary greatly, and the subjective weight values of P_3, S_2, I_1, and R_2 are heavier, and the objective weight values of D_1, P_4, S_4, I_2, and R_4 are heavier, which will result in large errors in actual calculations.

4.2.3. Game Combination Results

1. Calculate the weight linear coefficient

Through game combination weighting, the differences and conflicts between the two weighting methods can be well coordinated, making up for the incompleteness of a single weighting method. The weight value distribution coefficients of the assessment indexes are calculated according to Formulas (16)–(19) as shown in Table 7.

Table 7. Weight linear coefficient.

Indicator Layer	G1	CRITIC
First level indicator	0.7450	0.2550
Secondary indicators	0.9366	0.0634

2. Calculate the combined weight

Combining the basic principles and calculation steps of game theory, based on the MatlabR2024b software platform, the linear coefficients of the optimized combination weights are input, and finally the weights of the optimized combination are calculated according to Formula (20). The results are shown in Figure 11.

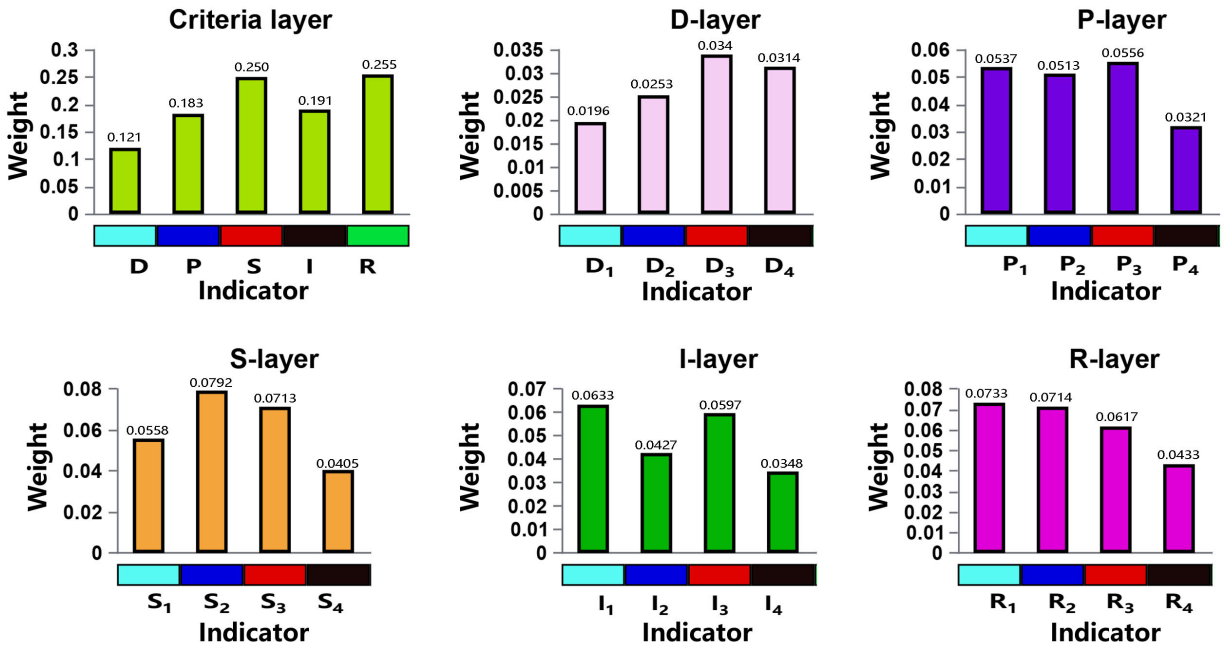


Figure 11. Combination weight.

From Figure 11, we can see that among the indicators in the criterion layer, R has the largest weight and P has the smallest weight. In the indicator layer, S_2 has the largest weight and D_1 has the smallest weight. In the indicator D layer, the weights are D_3, D_4, D_2, and D_1 from large to small. In the indicator P layer, the weights are P_3, P_1, P_2, and P_4 from large to small. In the indicator S layer, the weights are S_2, S_3, S_1, and S_4 from large to small.

In the indicator I layer, the weights are I_1, I_3, I_2, and I_4 from large to small. In the indicator R layer, the weights are R_1, R_2, R_3, and R_4 from large to small.

4.3. Results of the Improved Cloud Model

4.3.1. Cloud Digital Characteristics of Indicators

Five experts were invited to score each assessment indicator according to the assessment system established in Chapter 3.1.2. The expert questionnaire information is shown in Appendix C. The scoring results are shown in Figure 12. The figure contains five circles, each of which represents the score of an expert for the assessment indicator.

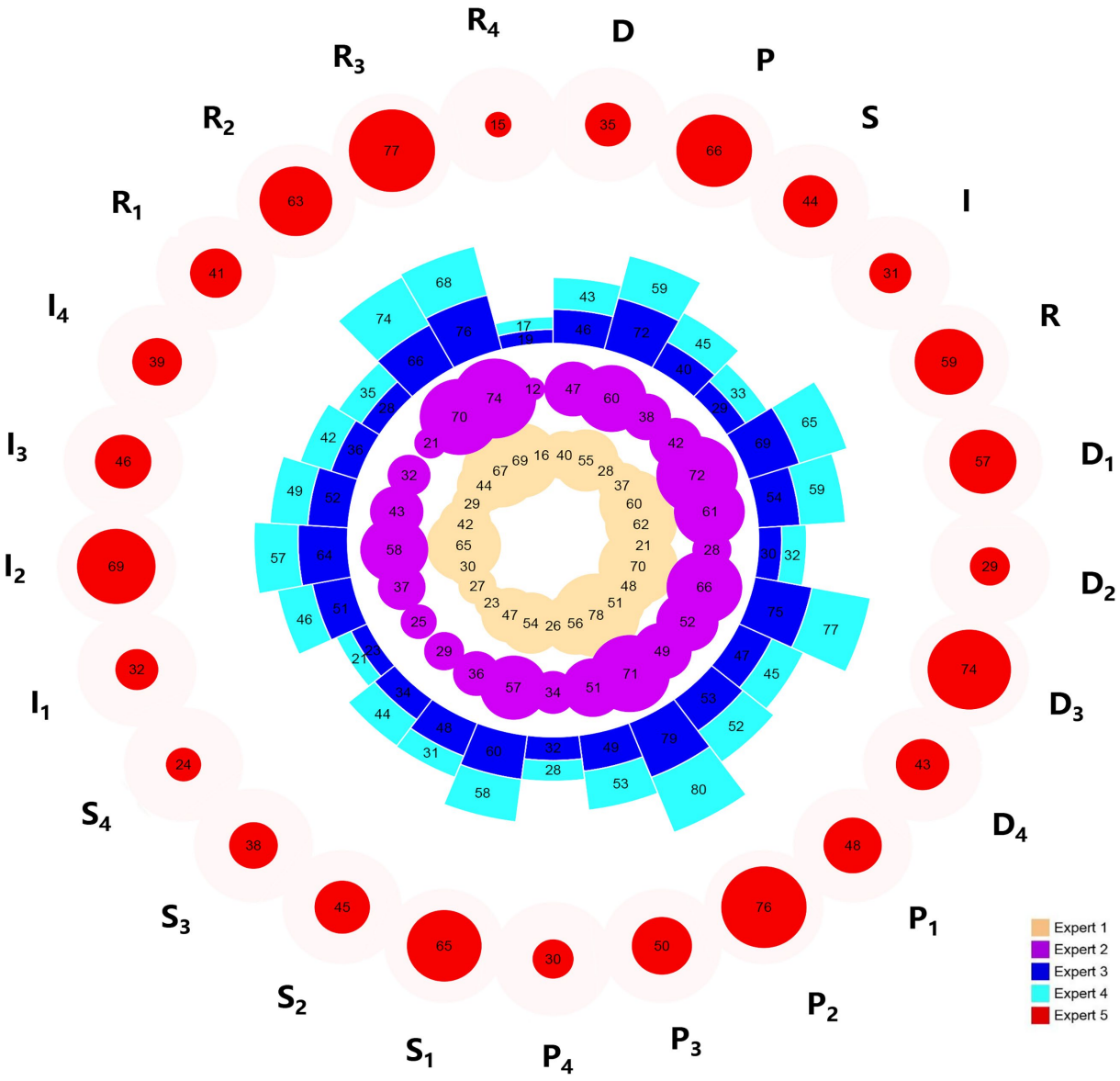


Figure 12. Expert scoring results.

Substitute the score values into Formulas (21)–(24) for calculation and determine the digital characteristics of the cloud model of the indicator layer factors of the assessment system, as shown in Table 8 The comprehensive clouds of the criterion layer and the indicator layer are (49.119, 15.536, 3.559), (45.894, 4.951, 1.621) respectively.

Table 8. Cloud digital characteristics of assessment indicators.

Indicator Layer	(*Ex*, *En*, *He*)
D	(44, 13.536, 2.953)
P	(51.8, 14.238, 2.552)
S	(51.2, 19.351, 5.076)
I	(49, 13.034, 1.974)
R	(47, 15.541, 3.609)
D_1	(58.6, 3.108, 0.799)
D_2	(28, 3.509, 2.277)
D_3	(72.4, 4.412, 0.403)
D_4	(47, 3.008, 1.566)
P_1	(50.6, 2.106, 0.365)
P_2	(76.8, 3.309, 1.324)
P_3	(51.8, 2.707, 0.609)
P_4	(30, 3.008, 0.976)
S_1	(58.8, 3.71, 1.714)
S_2	(41.4, 7.921, 2.538)
S_3	(33.6, 7.62, 2.689)
S_4	(24, 2.005, 0.989)
I_1	(39.2, 9.325, 2.291)
I_2	(62.6, 5.114, 0.921)
I_3	(46.4, 4.111, 0.633)
I_4	(35.6, 5.114, 1.073)
R_1	(33.8, 9.325, 1.323)
R_2	(68, 4.011, 1.19)
R_3	(72.8, 4.311, 1.374)
R_4	(15.8, 2.306, 1.176)

4.3.2. Computing Standard Cloud

The assessment level is divided into 5 levels, namely {Extremely weak, Weak, General, Strong, Extremely strong}. According to the toughness level assessment range, the assessment standard cloud characteristic parameters are calculated by Formula (25) and the final assessment result is compared and analyzed with it to determine the assessment level. The results are shown in Table 9.

Table 9. Standard cloud characteristic parameters.

Cloud Model Characteristic Parameters	*Ex*	*En*	*He*
Comment 1	12.5	4.167	0.5
Comment 2	37.5	4.167	0.5
Comment 3	62.5	4.167	0.5
Comment 4	82.5	2.5	0.5
Comment 5	95.0	1.667	0.5

4.3.3. Generate Indicator Layer, Criterion Layer and Comprehensive Assessment Cloud

Substitute the cloud digital features and game combination weights of the indicator layer and criterion layer of the assessment index into Formulas (26) and (27) to obtain the assessment cloud maps of the indicator layer and target layer. Use Matlab R2024b to draw the cloud maps of the standard cloud and the indicator layer and the criterion layer assessment index into the same coordinate system, as shown in Figure 13.

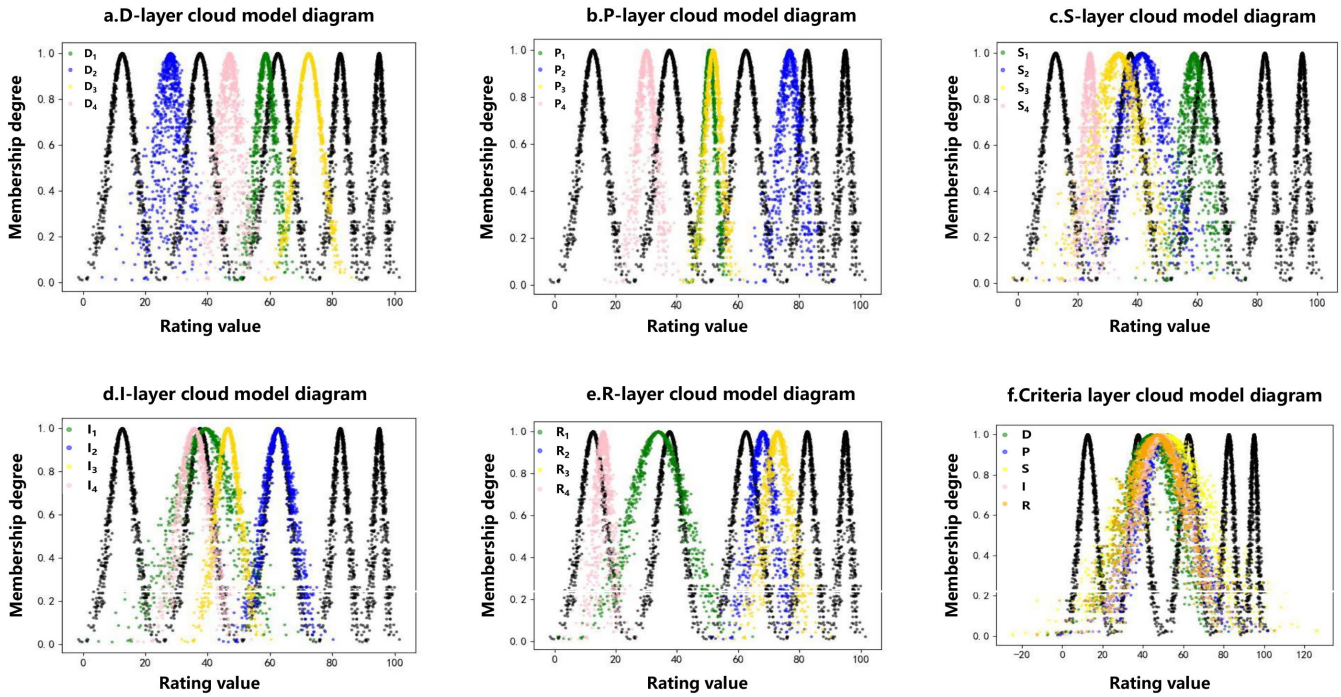


Figure 13. Cloud model diagram of the criteria layer and indicator layer.

From Figure 13a, we can see that the assessment result cloud map of the crowd condition (D_1) is between "General" and "Weak", closer to "General", so the assessment result of the number of rainstorm days in a year (D_1) is "General". Similarly, the assessment result of the block construction year (D_2) is "Weak", the assessment result of the number of rainstorm days in a year (D_3) is "Strong", and the assessment result of municipal facilities (D_4) is "Weak".

From Figure 13b, we can see that the assessment result cloud map of the rainstorm intensity (P_1) is between "general" and "Weak", closer to "General", and the assessment result is "General". Similarly, the assessment result of the flooding duration (P_2) is "Strong", the assessment result of the flooding depth (P_3) is "General", and the assessment result of the water flow velocity (P_4) is "Weak".

From Figure 13c, we can see that the cloud map assessment result of the impervious area of the catchment area (S_1) is "General ". The assessment result of the maximum water depth of the drainage well (S_2) is "weak", the assessment result of the total area of the catchment area (S_3) is "Weak", and the assessment result of the block road grade (S_4) is "Weak".

From Figure 13d, we can see that the cloud map assessment result of the current capacity (I_1) is "Weak". The assessment result of the outdoor property (I_2) is "General", the assessment result of the road accessibility (I_3) is "Weak", and the assessment result of the building structure (I_4) is "Weak".

From Figure 13e, we can see that the cloud map assessment result of the maximum flood flow of the drainage well (R_1) is "Weak", the assessment result of the rescue and evacuation capacity (R_2) is "General", the assessment result of the emergency plan (R_3) is "General ", and the assessment result of the number of shelters (R_4) is "Extremely weak".

As shown in Figure 13f, the cloud map assessment result of driving force (D) is "Weak". Similarly, the assessment result of pressure (P) is "General", the assessment result of state (S) is "General", the assessment result of impact (I) is "Weak", and the assessment result of response (R) is "Weak".

The comprehensive assessment cloud map calculated by Matlab R2024b using Formula (28) is closer to the "Weak" level, as shown in Figure 14.

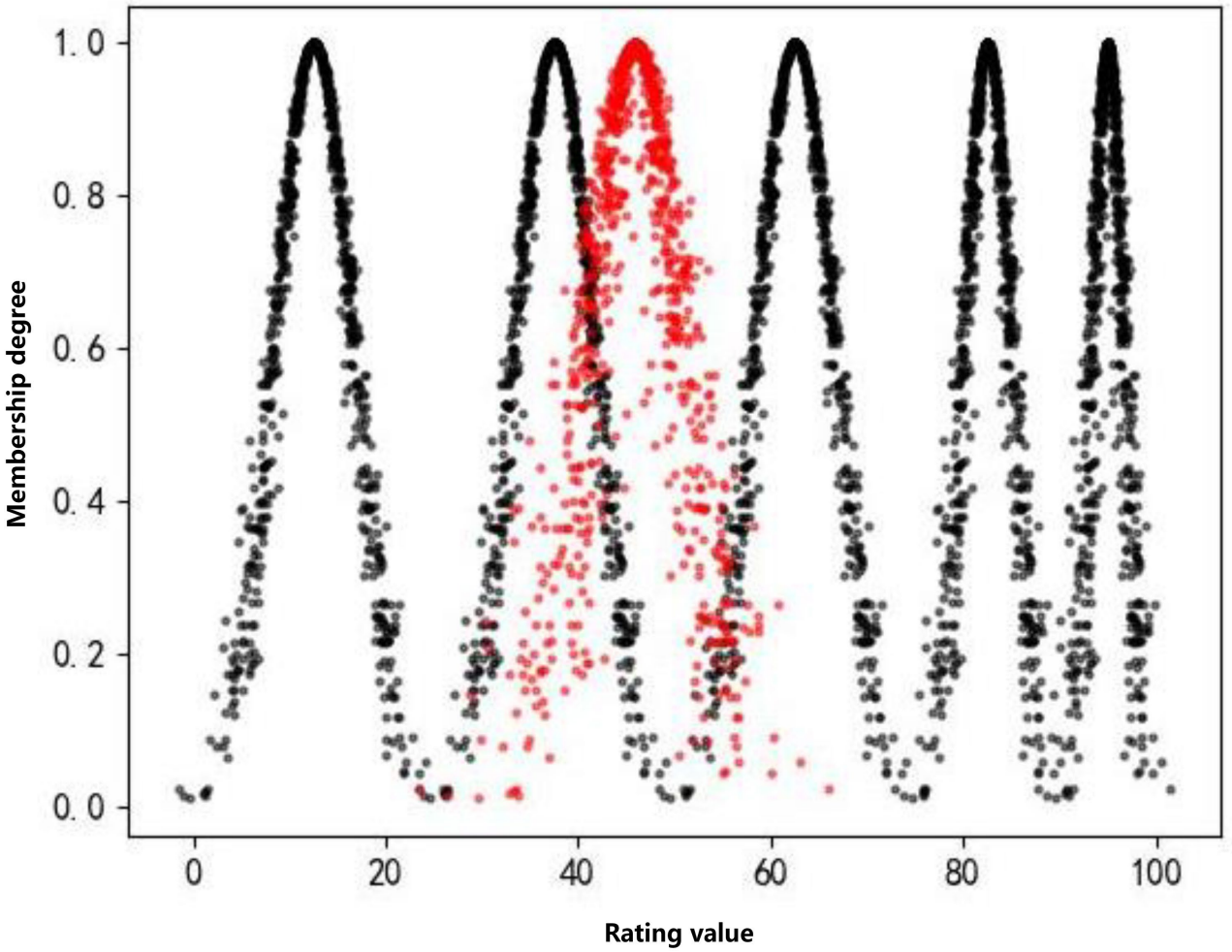


Figure 14. Cloud model diagram of standard cloud and comprehensive cloud.

4.3.4. Cloud Similarity Calculation Results

The index cloud similarity is calculated by Formulas (29)–(31) The calculation results are shown in Tables 10 and 11. It is found that the calculation results of cloud similarity are consistent with those obtained by the cloud map method.

Table 10. Criterion stratus cloud similarity calculation results.

Criteria Layer	Rank					Assessment Results
	Extremely Weak	Weak	General	Strong	Extremely Strong	
D	0.061	0.707	0.227	0.005	0.000	Weak
P	0.017	0.431	0.507	0.044	0.000	General
S	0.107	0.392	0.421	0.065	0.015	General
I	0.016	0.558	0.410	0.016	0.000	Weak
R	0.079	0.557	0.330	0.034	0.000	Weak

Table 11. Calculation results of index layer cloud similarity.

Indicator Layer	Rank					Assessment Results
	Extremely Weak	Weak	General	Strong	Extremely Strong	
D1	0.000	0.001	0.999	0.000	0.000	Weak
D2	0.000	0.848	0.000	0.000	0.000	Weak
D3	0.000	0.000	0.774	0.226	0.000	General
D4	0.000	0.931	0.069	0.000	0.000	Weak
P1	0.000	0.397	0.603	0.000	0.000	General
P2	0.000	0.000	0.133	0.867	0.000	Strong
P3	0.000	0.183	0.817	0.000	0.000	General
P4	0.014	0.986	0.000	0.000	0.000	Weak
S1	0.000	0.002	0.998	0.000	0.000	General
S2	0.006	0.931	0.063	0.000	0.000	Weak
S3	0.071	0.924	0.005	0.000	0.000	Weak
S4	0.769	0.231	0.000	0.000	0.000	Extremely Weak
I1	0.029	0.910	0.061	0.000	0.000	Weak
I2	0.000	0.000	0.999	0.000	0.000	General
I3	0.000	0.950	0.050	0.000	0.000	Weak
I4	0.002	0.998	0.000	0.000	0.000	Weak
R1	0.120	0.872	0.008	0.000	0.000	Weak
R2	0.000	0.000	0.004	0.010	0.000	Strong
R3	0.000	0.000	0.729	0.271	0.000	General
R4	0.999	0.000	0.000	0.000	0.000	Extremely Weak
Comprehensive Cloud	0.363	0.451	0.006	0.002	0.177	Weak

The cloud map of the comprehensive cloud assessment model and the similarity calculation together concluded that the flood disaster resilience assessment result of the historic district of the Soviet-style building complex of Daye Steel Plant in Huangshi is at the "Weak" level.

5. Discussion

The assessment results of the driving force layer and pressure layer were "Weak" and "General" respectively, indicating that the historic district of the Soviet-style building complex of Daye Steel Plant in Huangshi is at great risk of flood disasters. In order to reduce the risk, rainwater adaptation technology should be used to build an ecological rainwater collection ditch, a rainfall runoff treatment facility made of highly permeable ecological concrete, which can effectively reduce the peak flow of runoff, reduce the flow rate of water flow, and prolong the flow time of rainwater in the canal. the assessment result of the state layer is "Weak", indicating that the resistance capacity of the historic district of the Soviet-style building complex of Huangshi Daye Steel Plant needs to be improved when flood disasters occur. Therefore, two primary and secondary flood control channel systems can be built in this historic district. The assessment result of the impact layer is "Weak", indicating that the historic district of the Soviet-style building complex of Huangshi Daye Steel Plant will cause great damage to the surrounding environment when flood disasters occur. A comprehensive and systematic urban flood management system can be established using a digital management platform to achieve automatic remote monitoring and advanced management. Strengthen the construction of information collection, communication and network, flood control and drainage warning and forecasting systems around the districts, and provide basic information and management decision-making support for flood control

and waterlogging prevention in historic districts. The response layer assessment result is "General". This shows that the emergency response capability of the historic district of the Soviet-style building complex of Daye Steel Plant in Huangshi is strong when flood disasters occur. In order to minimize the losses, an emergency management mechanism and emergency plan with unified command, hierarchical responsibility, departmental collaboration, rapid response, orderly coordination and efficient operation of flood disasters in historic districts can be established. At the same time, the relevant functional departments are entrusted or designated to conduct disaster prevention and relief training for the heads and employees of the member units of the emergency command center; ensure that the transfer and assessment of the people in the district is completed quickly and smoothly.

At present, research on flood resilience assessment specifically targeting urban historic districts remains limited [10–20]. Most existing studies focus on broader scales, such as entire cities or general urban areas, rather than on distinct, historically significant zones. For instance, Nazari et al. [47] used an integrated model to evaluate and analyze the economic resilience and vulnerability of small towns under severe storm disasters. The study found that small counties have greater economic vulnerability than large counties. Pal et al. [48] established an urban flood assessment framework and used machine learning methods for simulation, but the cases selected in the study may not be applicable to other similar scenarios. Wang et al. [49] developed a flood risk assessment framework based on the scale of urban agglomerations. This assessment framework can effectively assess large-scale urban agglomerations, but it is not applicable to small-scale areas with historical heritage, such as historic districts. Hamidi et al. [50] employed the MOVE framework to assess flood vulnerability in northern Peshawar, Pakistan. They used structured questionnaires for data collection and ArcGIS 10.6 tools for analysis. Their findings indicated high levels of vulnerability across the study area and suggested that government and disaster management agencies could reduce flood risks through public education, training, and disaster mitigation initiatives.Wu et al. [51] proposed a model that coupled ontology and Bayesian network to evaluate and predict flood risks, and verified the results with actual records. Maru et al. [52] used GIS and AHP weighted overlay analysis to effectively identify areas with higher flood risks. These studies illustrate that current urban flood resilience assessments primarily rely on structured surveys, historic flood data, and GIS-based spatial analysis. Indicator weights are generally derived using subjective and objective methods, with final results often validated against historic events. However, the urban historic district is a small-scale area, and historical flood data in the area is rarely obtained. Therefore, in order to accurately evaluate the urban historic district, the game theory algorithm is used to optimize the combination of subjective and objective weights of the assessment indicators, avoiding a certain degree of subjectivity while taking into account the actual local conditions in the study area. The cloud similarity measurement is introduced into the cloud model to obtain an improved cloud model, which can not only intuitively display the assessment results, but also verify the accuracy of the results through cloud similarity calculation. Therefore, the research results can provide decision support for urban planners, heritage conservation agencies, and flood risk managers. Managers can analyze the flood resilience assessment results of historic districts using the G-IC model, proactively implement appropriate technical and intervention measures to effectively regulate areas with low resilience, and proactively respond to safety factors in historic districts based on local conditions.

This study uses the game combination empowerment-improved cloud model assessment method to establish the G-IC model for urban historical district resilience assessment, which can provide a relatively comprehensive analysis for flood prevention and control in historic districts. This study also has certain limitations. Although the selection of flood

disaster resilience assessment indicators for urban historic districts has been combined with theoretical literature screening and practical investigation, it may still lack comprehensiveness. It is hoped that more scholars will join the research on flood disaster resilience in urban historic districts to establish a more scientific assessment system. Construct a more professional and detailed academic model, conduct research from the micro level and spatiotemporal evolution, and apply more research results to the flood disaster resilience assessment of urban historic districts. Furthermore, this study did not incorporate historical flood impact data to compare and validate the resilience results. This could be incorporated into subsequent research to enhance the validity of the results. Flood disasters inevitably cause economic losses to historic districts, so analyzing flood resilience from the perspective of economic characteristics is crucial. Furthermore, analyzing the impact of architectural heritage characteristics on flood resilience within historic districts is an area that warrants further refinement in subsequent research.

6. Conclusions

There are a large number of unquantifiable qualitative factors in the influencing factors of flood disaster resilience assessment in urban historic districts, which causes the randomness and ambiguity of the assessment. This paper establishes a five-level index system for flood disaster resilience assessment in urban historic districts through DPSIR theory, field investigation and expert consultation. The established game combination empowerment-improved cloud model is applied to the flood disaster resilience assessment of the historic districts of the Soviet-style building complex of Daye Steel Plant in Huangshi. The following research conclusions were obtained.

(1) Based on the DPSIR model, an urban historic district flood disaster resilience assessment system was established, and the 20 screened and verified assessment indicators were divided into five indicator layers, thus obtaining a more comprehensive urban historic district flood disaster resilience assessment indicator system.

(2) The accuracy of the weight values of assessment indicators is increased by using game combination weighting. Considering the fuzziness and randomness of the flood disaster resilience assessment process of urban historic districts, an urban historic district flood disaster resilience assessment model based on game combination weighting-improved cloud model is constructed to improve the accuracy of the assessment.

(3) The G-IC model for flood disaster resilience assessment of urban historic districts was established. The assessment of the Soviet-style building complex of Daye Steel Plant in Huangshi showed that the resilience of the driving force layer was at the "Weak" level, the resilience of the pressure layer was at the "General" level, the resilience of the state layer was at the "General" level, the resilience of the influence layer was at the "Weak" level, and the resilience of the response layer was at the "Weak" level. The final result was "Weak" and the consistency of the results was verified by calculating the cloud similarity, indicating that the constructed new model has certain rationality and feasibility.

Author Contributions: Conceptualization, B.H.; methodology, B.H.; software, B.H.; validation, T.K.; formal analysis, B.H. and T.K.; investigation, B.H.; resources, B.H.; data curation, B.H.; writing—original draft preparation, B.H.; writing—review and editing, B.H. and G.Z.; visualization, B.H.; supervision, T.K. and G.Z.; project administration, B.H.; funding acquisition, B.H. All authors have read and agreed to the published version of the manuscript.

Funding: This research was funded by the China Scholarship Council (CSC) and Institute of Science Tokyo, grant number: 202406950135; the PhD Scientific Research and Innovation Foundation of Sanya Yazhou Bay Science and Technology City, grant number HSPHDSRF-2023-03-009. And the Hubei Natural Resources Science and Technology Project, grant number ZRZY2025KJ35. The support is

gratefully acknowledged. Any opinions, findings, conclusions, or recommendations expressed in this study are those of the authors and do not necessarily reflect the views of the sponsoring agencies.

Data Availability Statement: All data, models, or codes that support the findings of this study are available from the corresponding author upon reasonable request.

Conflicts of Interest: The authors declare no conflict of interest. The funders had no role in the design of the study; in the collection, analyses, or interpretation of data; in the writing of the manuscript; or in the decision to publish the results.

Appendix A. Questionnaire for Screening Indicators of Flood Disaster Resilience Assessment in UHD

Dear experts,

This questionnaire survey is intended to support my thesis research work. The information collected will be strictly confidential and does not involve any personal privacy or commercial sensitive content. Your answers will only be used for data analysis and research in this thesis, so please feel free to answer. This questionnaire survey is divided into three parts. Before filling in the questionnaire, you can read the relevant filling instructions first for effective scoring. Thank you very much for your support and help!

1. What type of work unit do you work for?

A. Colleges and universities B. Emergency departments C. Design institutes D. Research institutes E. Others

2. What is your job title?

A. Intermediate Engineer B. Senior Engineer C. Associate Professor

D. Professor E. Other

Please read the following materials and, based on your work experience and personal experience, judge whether the 24 influencing factors in Table A1 can be used as indicators for the flood disaster resilience rating assessment system for urban historic districts (each item can be abandoned). If you think there are other possible assessment indicators, please add them to Table A2 and explain the reasons.

Table A1. List of indicators for assessing the resilience of UHD to flood disasters.

Serial Number	Factors Affecting Indicators	Expert Rating				
		1	2	3	4	5
1	Crowd conditions					
2	Impervious area of catchment area					
3	Submerged duration					
4	Maximum flood flow of drainage well					
5	Emergency Plan					
6	Municipal facilities					
7	Submergence depth					
8	Year of block construction					
9	Road accessibility					
10	Block road grade					
11	Downstream flow capacity					
12	Authenticity					
13	Total catchment area					
14	Building Structure					

Table A1. *Cont.*

Serial Number	Factors Affecting Indicators	Expert Rating				
		1	2	3	4	5
15	Rainstorm days in the year					
16	Building Materials					
17	Number of evacuation sites					
18	Outdoor property					
19	Cultural uniqueness					
20	Water flow rate					
21	Rescue and evacuation capacity					
22	Maximum water depth of drainage well					
23	Heavy rain intensity					
24	The proportion of secondary output value					

Table A2. Additional items for the UHD flood disaster resilience assessment system indicator questionnaire.

Add Item	Add Reason	Add Item	Add Reason

Appendix B. Questionnaire on the Weights of Flood Disaster Resilience Assessment Indicators for UHD

Dear experts,

Thank you for taking the time to read this questionnaire in your busy schedule. Based on the previous survey results, 20 key assessment indicators were finally determined. Based on your professional knowledge and work experience, please assign values to the following assessment indicators and refer to Table A3, sort them from large to small according to your understanding of the importance, and number them in order from small to large, and fill in the corresponding values in the importance sorting column. Thank you again for your participation and support!

Table A3. Evaluation criteria for importance of assessment indicators.

R_z Value	Value Description
1.0	Indicator X_{z-1} is as important as X_z
1.1	Indicator X_{z-1} is equally important to slightly more important than X_z
1.2	Indicators X_{z-1} and X_z are slightly more important
1.3	The index X_{z-1} is between slightly important and important with respect to X_z
1.4	Indicator X_{z-1} is more important than X_z
1.5	The weight of indicator X_{z-1} and X_z is between important and obviously important
1.6	Indicators X_{z-1} and X_z are obviously important
1.7	The index X_{z-1} and X_z are between obviously important and strongly important
1.8	Indicators X_{z-1} and X_z are strongly important

Table A4. Comparison matrix of target layer assessment indicators.

Index	Sequence	Ratio 1	Ratio 2	Ratio 3	Ratio 4
Criteria Layer					

Table A5. Comparison matrix of indicator level assessment indicators.

Index	Sequence	Ratio 1	Ratio 2	Ratio 3
D-layer indicators				
P-layer indicators				
S-layer indicators				
I-layer indicators				
R-layer indicators				

Appendix C. Scoring Table for Flood Disaster Resilience Assessment Indicators for UHD

Dear experts,

Thank you for continuing to participate in the third part of the survey. We sincerely invite you to participate in this questionnaire. Please divide the level of resilience of urban historic districts to flood disasters reflected by the index layer influencing factors in the following Table A6 into 5 scoring levels, and score from 0 to 100, where [0, 25] indicates extremely weak resilience, (25,50] indicates weak resilience, (50,75] indicates average resilience, (75,90] indicates strong resilience, and (90,100] indicates extremely strong resilience. This article adopts the bilateral constraint scoring principle. Please choose the maximum and minimum scores in the appropriate interval for scoring and fill in the scores in Table A6. Thank you very much for your support and help!

Table A6. Scoring table for flood disaster resilience assessment indicators of UHD.

Criteria Layer	Fraction	Indicator Layer	Fraction
Driving force		Crowd conditions	
		Year of block construction	
		Rainstorm days in the year	
		Municipal facilities	
Pressure		Heavy rain intensity	
		Submerged duration	
		Submergence depth	
		Water flow rate	

Table A6. *Cont.*

Criteria Layer	Fraction	Indicator Layer	Fraction
State		Impervious area of catchment area	
		Maximum water depth of drainage well	
		Total catchment area	
		Block road grade	
Influence		Overcurrent capacity	
		Outdoor property	
		Road accessibility	
		Building Structure	
Response		Maximum flood flow of drainage well	
		Rescue and evacuation capacity	
		Emergency Plan	
		Number of evacuation sites	

References

1. Choi, S.; Walter, R.J.; Chalana, M. Untangling our checkered past: Investigating the link between local historic district designation and spatial segregation history. *Cities* **2025**, *158*, 105621. [CrossRef]
2. Escobedo, D.N. Foreigners as gentrifiers and tourists in a Mexican historic district. *Urban Stud.* **2020**, *57*, 3151–3168. [CrossRef]
3. Zhou, T.; Zhou, Y.; Liu, G. Comparison of critical success paths for historic district renovation and redevelopment projects in China. *Habitat Int.* **2017**, *67*, 54–68. [CrossRef]
4. Kuzulugil, A.C.; Ünsal, Ö.; Yildiz, N.D.; Aytatli, B. Space syntax-based analysis method to improve the accessibility of urban tourism in a historic environment. *J. Fac. Eng. Archit. Gazi Univ.* **2023**, *38*, 2359–2374. [CrossRef]
5. Li, M.; Liu, J.; Lin, Y.; Xiao, L.; Zhou, J. Revitalizing historic districts: Identifying built environment predictors for street vibrancy based on urban sensor data. *Cities* **2021**, *117*, 103305. [CrossRef]
6. Miranda, F.N.; Ferreira, T.M. A simplified approach for flood vulnerability assessment of historic sites. *Nat. Hazards* **2019**, *96*, 713–730. [CrossRef]
7. Fiori, A.; Mancini, C.P.; Annis, A.; Lollai, S.; Volpi, E.; Nardi, F.; Grimaldi, S. The role of residual risk on flood damage assessment: A continuous hydrologic-hydraulic modelling approach for the historical city of Rome, Italy. *J. Hydrol. Reg. Stud.* **2023**, *49*, 101506. [CrossRef]
8. Nguyen, T.L.; Asahi, C.; Tran, T.A.; Le, N.H. Indicator-based approach for flood vulnerability assessment in ancient heritage city of Hoi An, Central Region of Vietnam. *Nat. Hazards* **2022**, *114*, 2357–2385. [CrossRef]
9. D'Ayala, D.; Wang, K.; Yan, Y.; Smith, H.; Massam, A.; Filipova, V.; Pereira, J.J. Flood vulnerability and risk assessment of urban traditional buildings in a heritage district of Kuala Lumpur, Malaysia. *Nat. Hazards Earth Syst. Sci.* **2020**, *20*, 2221–2241. [CrossRef]
10. Kittipongvises, S.; Phetrak, A.; Rattanapun, P.; Brundiers, K.; Buizer, J.L.; Melnick, R. AHP-GIS analysis for flood hazard assessment of the communities nearby the world heritage site on Ayutthaya Island, Thailand. *Int. J. Disaster Risk Reduct.* **2020**, *48*, 101612. [CrossRef]
11. Bomers, A.; Van der Meulen, B.; Schielen, R.M.J.; Hulscher, S.J.M.H. Historic flood reconstruction with the use of an artificial neural network. *Water Resour. Res.* **2019**, *55*, 9673–9688. [CrossRef]
12. Aktürk, G.; Hauser, S.J. Detection of disaster-prone vernacular heritage sites at district scale: The case of Fındıklı in Rize, Turkey. *Int. J. Disaster Risk Reduct.* **2021**, *58*, 102238. [CrossRef]
13. Pala, O.N.; Cetinkaya, I.D.; Yazar, M. Urban Flood Exposure and Vulnerability: Insights From Pendik District of Istanbul. *J. Flood Risk Manag.* **2025**, *18*, e70000. [CrossRef]
14. Seo, S.B.; Jee, H.W.; Cho, J.; Oh, C.; Chae, Y.; Jo, S.; Hur, J. Assessment of the flood damage reduction effect of climate change adaptation policies under temperature increase scenarios. *Mitig. Adapt. Strat. Glob. Change* **2024**, *29*, 8. [CrossRef]

15. Salazar, L.G.F.; Figueiredo, R.; Romão, X. Flood vulnerability assessment of built cultural heritage: Literature review and identification of indicators. *Int. J. Disaster Risk Reduct.* **2024**, *111*, 104666. [CrossRef]
16. Pei, W.; Tian, C.; Fu, Q.; Ren, Y.; Li, T. Risk analysis and influencing factors of drought and flood disasters in China. *Nat. Hazards* **2022**, *110*, 1599–1620. [CrossRef]
17. Owuor, M.O.; Mwiturubani, D.A. Correlation between flooding and settlement planning in Nairobi. *J. Water Clim. Change* **2022**, *13*, 1790–1805. [CrossRef]
18. Karimi Sangchini, E.; Salehpour Jam, A.; Mosaffaie, J. Flood risk management in Khorramabad watershed using the DPSIR framework. *Nat. Hazards* **2022**, *114*, 3101–3121. [CrossRef]
19. Deng, W.; Li, M.; Guo, Y. Research on fuzzy evaluation of ecological safety of land resources in Pearl river Delta area based on DPSIR framework. *Sci. Rep.* **2025**, *15*, 8059. [CrossRef]
20. Jam, A.S.; Mosaffaie, J.; Tabatabaei, M.R. Assessment of comprehensiveness of soil conservation measures using the DPSIR framework. *Environ. Monit. Assess.* **2021**, *193*, 42. [CrossRef]
21. Li, Q.; Liu, Z.; Yang, Y.; Han, Y.; Wang, X. Evaluation of water resources carrying capacity in Tarim River Basin under game theory combination weights. *Ecol. Indic.* **2023**, *154*, 110609. [CrossRef]
22. Liu, J.; Li, Y.; Lu, Y.; Fu, X.; Yan, S. Research on the influence factors of ubiquitous power Internet of things for promoting consumption of wind power based on fuzzy G1-ISM in China. *Int. J. Electr. Power Energy Syst.* **2020**, *121*, 106124. [CrossRef]
23. Ye, F.; Sun, J.; Wang, Y.; Nedjah, N.; Bu, W. A novel method for the performance evaluation of institutionalized collaborative innovation using an improved G1-CRITIC comprehensive evaluation model. *J. Innov. Knowl.* **2023**, *8*, 100289. [CrossRef]
24. Ma, W.; Xiao, C.; Ahmed, S.F.; Feng, T.; Liu, G. Multi-objective carbon neutrality optimization and G1-EW-TOPSIS assessment for renewable energy transition. *J. Clean. Prod.* **2023**, *415*, 137808. [CrossRef]
25. Li, G.; Wang, H.; Pan, T.; Liu, H.; Si, H. Fuzzy comprehensive evaluation of Pilot Cadets' flight performance based on G1 method. *Appl. Sci.* **2023**, *13*, 12058. [CrossRef]
26. Yu, X.; Suntrayuth, S.; Carayannis, E.G.; Sindakis, S.; Showkat, S. Advancing industrial wastewater treatment through comprehensive evaluation and innovative technology: A G1-entropy improved TOPSIS model approach. *J. Technol. Transf.* **2023**, *48*, 1–31. [CrossRef]
27. Zhang, Q.; Liu, C.; Guo, S.; Wang, W.; Luo, H.; Jiang, Y. Evaluation of the rock burst intensity of a Cloud Model based on the CRITIC method and the Order Relation Analysis Method. *Min. Metall. Explor.* **2023**, *40*, 1849–1863. [CrossRef]
28. Wen, X.; Nie, Y.; Du, Z.; Huang, L. Operational safety assessment of straddle-type monorail vehicle system based on cloud model and improved CRITIC method. *Eng. Fail. Anal.* **2022**, *139*, 106463. [CrossRef]
29. Mishra, A.R.; Chen, S.M.; Rani, P. Multicriteria decision making based on novel score function of Fermatean fuzzy numbers, the CRITIC method, and the GLDS method. *Inf. Sci.* **2023**, *623*, 915–931. [CrossRef]
30. Liu, X.; Wang, Z.; Pan, D.; Zhang, Y.; Zhang, J.; Chen, Y. Evaluation of Operational Safety Risk in Wastewater Treatment Plants Based on WSR and Matter–Element Extension Theory. *Water* **2024**, *16*, 2925. [CrossRef]
31. Wu, M.; Chen, M.; Chen, G.; Zheng, D.; Zhao, Y.; Wei, X.; Xin, Y. Research on methodology for assessing social vulnerability to urban flooding: A case study in China. *J. Hydrol.* **2024**, *645*, 132177. [CrossRef]
32. Zou, Q.; Liao, L.; Qin, H. Fast comprehensive flood risk assessment based on game theory and cloud model under parallel computation (P-GT-CM). *Water Resour. Manag.* **2020**, *34*, 1625–1648. [CrossRef]
33. Dai, H. Game Theory Combined Empowerment-Cloud Evaluation System. *Procedia Comput. Sci.* **2025**, *261*, 440–449. [CrossRef]
34. Peng, T.; Deng, H.; Lin, Y.; Jin, Z. Assessment on water resources carrying capacity in karst areas by using an innovative DPESBRM concept model and cloud model. *Sci. Total Environ.* **2021**, *767*, 144353. [CrossRef] [PubMed]
35. Hu, C.; Wang, Y.; Xia, G.; Han, Y.; Ma, X.; Liu, X. Health assessment method of cave murals based on entropy-weighted AHP-cloud model. *npj Heritage Sci.* **2025**, *13*, 279. [CrossRef]
36. Zhang, Y.; Hu, X.; Zhao, Z.; Gao, S.; Lv, M.; Jia, C.; Yang, X. Revealing hidden risks: Advanced assessment of urban land subsidence. *Earth Sci. Inform.* **2025**, *18*, 342. [CrossRef]
37. Lu, J.; Liu, J.; Su, X. A resilience evaluation method considering functional and structural resilience of urban drainage systems. *Urban Water J.* **2025**, *22*, 372–384. [CrossRef]
38. Guan, D.; Cao, J.; Huang, D.; Zhou, L. Early warning level identification and evolutionary trend prediction of ecological risk in the upper Chang Jiang (Yangtze R.), China. *Front. Earth Sci.* **2025**, *19*, 149–167. [CrossRef]
39. Chen, H.; Shen, G.Q.; Feng, Z.; Liu, Y. Assessment of the vulnerability of urban metro to rainstorms based on improved cloud model and evidential reasoning. *Tunn. Undergr. Space Technol.* **2025**, *157*, 106353. [CrossRef]
40. Zhang, R.; Yan, H. Complex system risk assessment model based on improved cloud DEMATEL-TAISM. *Civ. Eng. Environ. Syst.* **2025**, *42*, 32–55. [CrossRef]
41. Guan, X.; Liu, Y.; Meng, Y.; Wang, H.; Liu, M. Risk Assessment of Flood Disaster in Cities Based on "Disaster-Pregnant, Disaster-Causing, Disaster-Forming and Disaster-Curing". *Water Resour. Manag.* **2025**, *39*, 1521–1549. [CrossRef]

42. Yuan, D.; Xue, H.; Du, M.; Pang, Y.; Wang, J.; Wang, C.; Song, X.; Wang, S.; Kou, Y. Urban waterlogging resilience assessment based on combination weight and cloud model: A case study of Haikou. *Environ. Impact Assess. Rev.* **2025**, *111*, 107728. [CrossRef]
43. Cai, Y.; Chen, C.; Shi, Y.; Liu, R.; Wang, X.; Tao, X.; Yang, D. GIS and hybrid multi-criteria decision analysis based urban flood risk assessment in Hanchuan City, Hubei Province, China. *Environ. Earth Sci.* **2024**, *83*, 627. [CrossRef]
44. Hu, J.; Wang, F.; Liu, P.; Lü, S.; Lü, C.; Yu, F. Evaluation of urban water cycle health status based on DPSIRM framework and AHP-FCE-Cloud model. *Ecol. Indic.* **2025**, *170*, 112935. [CrossRef]
45. Liu, X.; Huang, H.; Wang, D.; Wu, Z.; Chen, P.; Ding, S.; Liang, X.; Yang, T. Robust multi-source forest point cloud registration with distribution similarity analysis. *IEEE Trans. Geosci. Remote Sens.* **2025**, *63*, 5701916. [CrossRef]
46. Pu, J.; Liu, Z. HECM-Plus: Hyper-Entropy Enhanced Cloud Models for Uncertainty-Aware Design Evaluation in Multi-Expert Decision Systems. *Entropy* **2025**, *27*, 475. [CrossRef] [PubMed]
47. Nazari, R.; Karimi, M.; Nikoo, M.R.; Khoshkonesh, A.; Museru, M.L. Can small towns survive climate change? Assessing economic resilience and vulnerability amid major storms. *J. Clean. Prod.* **2025**, *498*, 145158. [CrossRef]
48. Pal, L.; Saksena, S.; Dey, S.; Merwade, V.; Ojha, C.S.P. An integrative framework for assessment of urban flood response to changing climate. *Water Resour. Res.* **2023**, *59*, e2023WR034466. [CrossRef]
49. Wang, Y.; Zhang, Q.; Lin, K.; Liu, Z.; Liang, Y.-S.; Liu, Y.; Li, C. A novel framework for urban flood risk assessment: Multiple perspectives and causal analysis. *Water Res.* **2024**, *256*, 121591. [CrossRef]
50. Hamidi, A.R.; Wang, J.; Guo, S.; Zeng, Z. Flood vulnerability assessment using MOVE framework: A case study of the northern part of district Peshawar, Pakistan. *Nat. Hazards* **2020**, *101*, 385–408. [CrossRef]
51. Wu, Z.; Shen, Y.; Wang, H.; Wu, M. Urban flood disaster risk evaluation based on ontology and Bayesian Network. *J. Hydrol.* **2020**, *583*, 124596. [CrossRef]
52. Maru, D.R.; Kumar, V.; Sharma, K.V.; Pham, Q.B.; Patel, A. Integrating GIS, MCDM, and Spatial Analysis for Comprehensive Flood Risk Assessment and Mapping in Uttarakhand, India. *Geol. J.* **2025**, *60*, 2263–2280. [CrossRef]

Disclaimer/Publisher's Note: The statements, opinions and data contained in all publications are solely those of the individual author(s) and contributor(s) and not of MDPI and/or the editor(s). MDPI and/or the editor(s) disclaim responsibility for any injury to people or property resulting from any ideas, methods, instructions or products referred to in the content.